Polysaccharide-based aerogels for thermal insulation and superinsulation: An overview

Fangxin Zou, Tatiana Budtova

Polysaccharide-based aerogels for thermal insulation and superinsulation: an overview

Fangxin Zou, Tatiana Budtova*

MINES ParisTech, PSL Research University, Center for Materials Forming (CEMEF), UMR CNRS 7635, CS 10207, 06904 Sophia Antipolis, France

*Corresponding author: Tatiana Budtova, Tatiana.budtova@mines-paristech.fr

Abstract

To reduce energy losses due to the insufficient thermal insulation is one of the current “hot” topics. Various commercial porous materials are used with the best conductivity around 0.03 – 0.04 W/(m·K). Aerogels are the only known materials with “intrinsic” thermal superinsulating properties, i.e. with thermal conductivity below that of air in ambient conditions (0.025 W/(m·K)). The classical thermal superinsulating aerogels are based on silica and some synthetic polymers, with conductivity 0.014 – 0.018 W/(m·K). Aerogels based on natural polymers are new materials created at the beginning of the 21st century. Can bio-aerogels possess thermal superinsulating properties? What are the bottlenecks in the development of bio-aerogels as new high-performance thermal insulation materials? We try to answer these questions by analyzing thermal conductivity of bio-aerogels reported in literature.

Key-words: cellulose; chitosan; pectin; alginate; starch; thermal conductivity; thermal insulation; density; specific surface area

1. Introduction

Insufficient thermal insulation leads to huge energy losses inducing massive energy consumption and greenhouse gas emissions. To solve this problem, thermal insulation needs to be improved which is usually done by using various porous materials. If willing to decrease the thickness of the insulating layer, high performance materials with the lowest possible thermal conductivity are required. The best commercial insulating materials, such as mineral wool and polymer foams, have thermal conductivity around 0.030 – 0.040 W/(m·K) (Alam, Singh, & Limbachiya, 2011). The family of the most performing materials and components with thermal conductivity below that of air in ambient conditions (0.025 W/(m·K)) are the *superinsulating* materials. Vacuum insulation panels possess the lowest conductivity, around 0.007 – 0.008 W/(m·K), but they are still of rather high cost and with problems related to aging and mechanical damage (Alam et al., 2011). Till now, only aerogels are known to be “intrinsically” thermal superinsulating materials at the atmospheric pressure due to their mesoporosity (pore size from 2 to 50 nm) and low density (around 0.1 g/cm^3). The lowest values of the thermal conductivity were obtained for silica and resorcinol-formaldehyde aerogels, around 0.012 – 0.015 W/(m·K) (see, for example, Koebel, Rigacci, & Achard (2012); Lu et al. (1992)), which decreases by more than half the thickness of the insulation layer as compared to the commercial materials (Alam et al., 2011). These extraordinary properties make aerogels very attractive materials for thermal insulation in buildings, pipe lines, aerospace, appliances and transport, boosting current research and development towards the improvement of aerogels’ properties and decrease of their price (Koebel, Huber, Zhao, & Malfait, 2016). Some metal oxide aerogels possess enhanced heat resistance properties at high temperatures with thermal conductivity down to 0.05 W/(m·K) (see, for example, Zu et al., 2014)

It is important to first define the term “aerogel”. IUPAC Gold Book describes an aerogel as “a gel

comprised of a microporous solid in which the dispersed phase is a gas" (IUPAC. Compendium of Chemical Terminology 2014). This definition is rather restrictive as it includes the materials only with pore sizes below 2 nm, thus excluding even classical silica aerogels which are mesoporous. It should also be noted that in our days the term "aerogels" is somehow overused as various types of low-density porous materials, even with low specific surface area and pores of diameter of several tens and hundreds of microns, are called aerogels. Porous materials as expanded polystyrene or polyurethane foam are not aerogels. As agreed between aerogel scientists, aerogels are dry open pores nanostructured (mesoporous with small macropores) materials with high porosity (above 90%) and high specific surface area (at least above 100 m^2/g but no formal agreement exists (Pierre, 2011; Ganesan et al., 2018; Budtova et al., 2020).

In general, aerogels are obtained from gels that are dried in supercritical conditions in order to preserve gel morphology (Figure 1). It is also possible to obtain high specific surface area materials using freeze-drying, but those are exceptional cases. In the following, gels that are freeze-dried will be called "cryogels" (sometimes called "foams" in literature) (Figure 1). Finally, gels that are dried either under ambient conditions or low vacuum will be called "xerogels" (Figure 1). In most cases, under these drying conditions a gel loses its porosity because of structure collapse. Here again there are exceptional cases when functionalization of the gel network helps the preservation of gel morphology after ambient pressure drying; the well-known case is silylation of silica gels resulting in a material with aerogel-like morphology and properties (Schwertfeger, Frank, & Schmidt, 1998).

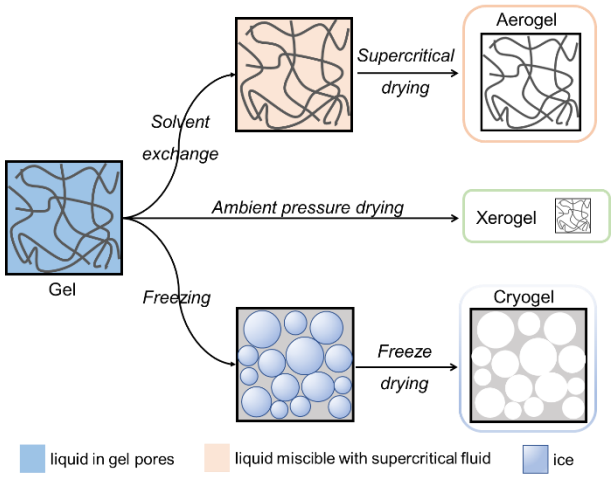

Figure 1.

Schematic presentation of the preparation of aerogels, xerogels, and cryogels from a gel.

Various matters (silica and metal oxides, monomers-precursors of synthetic polymers) have been used to synthesise aerogels; for the detailed information see Aerogels Handbook, 2011. In addition to low thermal conductivity, aerogels are suggested to be used for oil/water separation (Wang X. et al., 2020; Zou, Peng, Fu, Zhang, & Li, 2015), drug release (Follmann et al., 2020; Lim et al., 2020), energy storage (Lin et al., 2018; Zhou et al., 2018), for adsorption (Maleki, Whitmore, & Hüsing, 2018) and as catalyst supports (Wang M. et al., 2020; Zhang et al., 2017). At the beginning of the 21st century, a new class of aerogels was made: they are based on natural polymers such as polysaccharides and proteins (Zhao, Malfait, Guerrero-Alburquerque, Koebel, & Nyström, 2018; Budtova et al., 2020). Since the past 15 years the interest to bio-aerogels grew rapidly. One of the reasons is the use of renewable resources in order to reduce the environmental impact of synthetic polymer industry and move towards more sustainable society. Another reason is that bio-aerogels are biodegradable and often biocompatible which makes them very promising for biomedical applications. Finally, bio-aerogels can potentially be used in the same applications as classical aerogels: for separation, gas sorption, filtration, catalysts

and energy. The obvious “hot” question is “can a bio-aerogel be a thermal superinsulating material?” Literature reports on the thermal conductivity of various bio-aerogels but a systematic analysis summarizing the main trends and open questions is missing; an overview would help in moving forward (or not) towards bio-aerogels’ application for thermal insulation.

In this review, we focus on the relationships between the thermal conductivity and properties of aerogels based on polysaccharides. In some cases, the results on the thermal conductivity of bio-cryogels and bio-xerogels are included for the comparison. We do not discuss the overall properties and applications of each type of polysaccharide aerogel as each deserves a separate review article (see, for example, reviews on nanocellulose aerogels and foams (De France, Hoare, & Cranston, 2017; Lavoine & Bergström, 2017; Sun, Chu, Wu, & Xiao, 2021), on cellulose II aerogels (Budtova, 2019) and on starch aerogels (Zhu, 2019)). We start with the background on the thermal conductivity of porous materials and methods to obtain bio-aerogels and their characterization. Subsequently, we overview the current status of the thermal conductivity of aerogels based on cellulose, chitin and chitosan, pectin, starch and alginate. Finally, problems and prospects related to bio-aerogels’ applications for thermal insulation are discussed.

2. Background on the thermal conductivity of porous materials

The thermal conductivity (λ) of an isotropic porous material is, in the first approximation, a sum of gas (λ_g), solid (λ_s) and radiation (λ_r) components:

$$\lambda = \lambda_s + \lambda_g + \lambda_r \quad (1)$$

In general, heat transfer by convection should have also been taken into account but this term is negligible when the size of the pores is smaller than around 1 mm.

Thermal conductivity of a solid phase refers to the heat transfer along the network structure of a porous material and it is mainly affected by density. For example, for monolithic resorcinol-formaldehyde aerogels and their carbons the relationship between λ_s and aerogel bulk density ρ_{bulk} was shown to be described by power law (Lu et al., 1992; Lu, Nilsson, Fricke, & Pekala, 1993):

$$\lambda_s = C{\rho_{bulk}}^a \quad (2)$$

where C is the thermal conductivity of the backbone matter and a is a scaling exponent, usually around 1.2 – 2 (see, for example, Ebert, 2011). Therefore, one way to decrease the thermal conductivity of aerogel is to decrease its density.

Gas thermal conductivity refers to the heat transfer though the gaseous phase. At a given temperature and pressure, the main factors affecting λ_g are porosity ϕ and pore size D; convection can be neglected (Reichenauer, Heinemann, & Ebert, 2007; Wiener, Reichenauer, Braxmeier, Hemberger, Weis, Reichenauer, & Ebert, 2009) :

$$\lambda_g = \frac{\phi\lambda_{g0}}{1+2\beta l/D} \quad (3)$$

where λ_{g0} is the thermal conductivity of the free gas, β is a constant value related to the interactions between pore walls and gas molecules and is usually around 1.5 and l is the average free path of the gas molecule (around 70 nm for the air in ambient conditions). For a material of a given porosity, gas thermal conductivity can be decreased by decreasing pore diameter, and below l value λ_g may become lower than λ_{g0} (Knudsen effect). For example, it was demonstrated that decreasing pore diameter of a carbon aerogel from 10 μm to 200 nm, λ_g measured in argon at 0.1 MPa and 300 °C can be reduced from around 0.05 to 0.015 W/(m·K) (Hembergee, Weis, Reichenauer, & Ebert, 2009).

Radiation thermal conductivity λ_r depends on the optical thickness of the porous material. For optically thick aerogels, radiation thermal conductivity refers to the heat transfer due to the diffusion of

photons and can be described as follows:

$$\lambda_r = \frac{16\sigma n^2 T^3}{3\rho e} \quad (4)$$

where n is the effective refractive index of the porous material, σ is Stefan-Boltzmann constant (5.67×10^{-8} W·m^{-2}·K^{-4}), T is the temperature, and e is specific extinction coefficient which depends on the chemical composition and structure of the material and is inversely proportional to phonon mean free path. Therefore, λ_r strongly increases with temperature and decreases with the density. To decrease the radiation thermal conductivity, so-called infra-red opacifiers are sometimes added in a small quantity (in order not to increase aerogel density): they are highly absorbing or scattering particles, such as carbon black or titanium dioxide. In general, in optically thick porous materials the photon mean free path is very small compared to the thickness of the sample, and at not elevated temperature the radiation thermal conductivity is usually low.

Summarizing, in order to obtain a porous material with the lowest possible thermal conductivity (in particular, a thermal superinsulating material), a compromise between the density (to get low λ_s) and pore size (to gel low λ_g) is needed. Each input is counterbalancing the other, as shown in Figure 2. The minimum on this U-type curve is the ultimate value which is usually searched when making a thermal insulating and superinsulating material. Low solid conductivity can be provided by low density; for a porous material it is usually reached by decreasing the concentration of the matter which makes the network. However, this usually increases the size of the pores. To have pores' dimensions below 70 nm (mean free pass of air molecule) in a material filled with air in ambient conditions is the prerequisite for having λ_g lower than that of free air. This is the condition to obtain a superinsulating material. To make a low-density material with pores of such low dimensions is not straightforward, and thus most of the best thermal insulating foams possess thermal conductivity above that of air, around 0.030 – 0.035

W/(m·K). The main reason is too large pores, much above 70 nm. Numerous process parameters, such as matter type and concentration, mechanisms of network formation, way of solvent exchange (if applicable) and gel drying influence porous materials' morphology in which porosity, pore size and pore wall thickness are the key features influencing thermal conductivity. As explained in the next section, till now there is no standard method for measuring pore size distribution in bio-aerogels; thus, other indirect characteristics are needed to judge on bio-aerogels' pore dimensions. One of the criteria reflecting a large number of mesopores is high specific surface area. In the following, thermal conductivity of bio-aerogels will be analysed and correlated with material density and specific surface area.

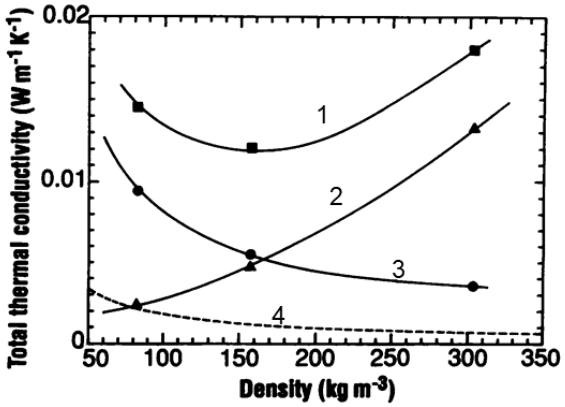

Figure 2.

Example of the thermal conductivity of resorcinol-formaldehyde aerogels: (1) total conductivity, (2) solid, (3) gaseous and (4) radiative (calculated). From Lu, X., Arduini-Schuster, M. C., Kuhn, J., Nilsson, O., Fricke, J., & Pekala, R. W. (1992). Thermal conductivity of monolithic organic aerogels. *Science*, *255*, 971–972. Reprinted with permission from AAAS

3. Preparation and characterization of aerogels, cryogels and xerogels based on polysaccharides

Bio-aerogels are prepared by polymer dissolution (except the case of nanocellulose and nanochitin), solution gelation (in some cases this step can be omitted), and drying which preserves network morphology, usually with supercritical CO_2 (Figure 3). Opposite to dissolved polysaccharides (Figure 3a), nanocellulose and nanochitin make suspensions of nanofibrils or nanocrystals (Figure 3b), usually dispersed in water. In all the cases, the preparation of bio-aerogels is fundamentally different from the synthesis of silica- or synthetic polymer-based aerogels which is starting with the polymerization of monomers. As most of polysaccharide solvents are not miscible with CO_2, solvent exchange step is needed. Ethanol or acetone are used for this purpose, and in the majority of cases they are polysaccharides' anti-solvents. Two different mechanisms of structure formation in aerogel precursor before drying are possible: direct non-solvent induced phase separation if solution was not gelled, or gelation (Figure 3a). Opposite to many synthetic polymer-based gels that are collapsing in a non-solvent, polysaccharide solutions and gels are shrinking to a certain extent during solvent exchange, but they still keep a 3D shape and porosity.

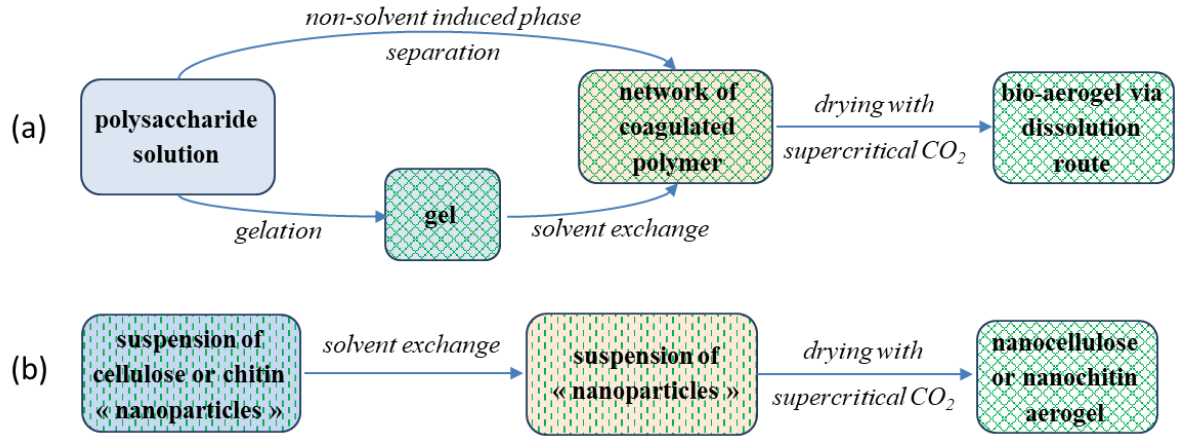

Figure 3.

Schematic presentation of the preparation of bio-aerogels: from polysaccharide solution (a) and from suspension (b).

Drying is a challenging final step in the preparation of bio-aerogels as it should preserve network morphology and avoid pores' collapse. During drying, a meniscus of the evaporating fluid is formed within the pores of the network and capillary pressure P develops; it depends on the surface tension γ of the evaporating liquid, angle θ between the liquid forming meniscus and the pore wall and pore radius r:

$$\mathrm{P} = \frac{2\gamma cos\theta}{r} \quad (5)$$

Drying in supercritical conditions is, till now, the best way to preserve gel morphology as no meniscus is formed and the capillary pressure is theoretically zero. CO_2 in the supercritical state is the most often used substance thanks to its mild critical temperature (31.3 °C) and pressure (72.9 atm).

Another way to avoid capillary pressure is to freeze the liquid in the pores of the network and then perform sublimation. The conventional procedure is freezing water in the pores of a gel; freezing usually results in very large macropores that are replicas of ice crystals. Two main approaches are used, random freezing resulting in no preferential pores orientation, and ice-templating resulting in the formation of elongated pores and channels (Figure S1 in the Supporting Information). As it will be shown in the following, freeze-drying is widely used to produce nanocellulose-based cryogels (or foams). If willing to preserve gel morphology, the kinetics of ice crystals growth must be controlled which can be done by either spray-freeze-drying which allows fast freezing resulting in sub-micron size pores, or by using mixed solvents.

Ambient pressure or low vacuum evaporative drying usually does not preserve gel morphology due to the high capillary pressure (eq. 5); xerogels with rather high density and low specific surface area are formed. In rare cases, polysaccharides with certain meso- and macroporosity can be obtained if the liquid in the network pores is with low surface tension; in this case solvent exchange step(s) are needed.

Bio-aerogels are characterized using the same methods as for inorganic and synthetic polymer aerogels, but certain precautions must be taken in order not to obtain the artefacts. The first problem is high hydrophilicity of native polysaccharides. Adsorption of water vapours may influence all characteristics, from density to specific surface area and also mechanical and thermal properties. Subsequent drying of a bio-aerogel which was exposed to humidity may not help as evaporative drying usually leads to the irreversible pores' closure; for cellulose this phenomenon is called "hornification". "Post-drying" may lead to aerogel shrinkage and change of density, morphology and, as a consequence, of all other properties. The conditions of samples' storage are thus very important but, unfortunately, are rarely reported. The aging of bio-aerogels is practically not studied.

Bulk (or apparent) density ρ_{bulk} is usually determined by measuring sample weight and volume, the latter is often calculated from sample's dimensions. For samples with geometrically complex shapes a powder densitometer, such as Geopyc from Micromeritics with DryFlo powder, is a useful option (Demilecamps, Beauger, Hildenbrand, Rigacci, & Budtova, 2015; Rudaz et al., 2014). Skeletal density $\rho_{skeletal}$ of polysaccharides is known to be 1.5 – 1.7 g/cm^3.

High resolution scanning electron microscopy (SEM) is a perfect tool to visualize aerogel morphology, but cannot be used to quantitatively describe it. Specific surface area S_{BET}, obtained using nitrogen adsorption technique and Brunauer–Emmett–Teller (BET) theory, is one of the main parameters characterizing aerogel texture. Unfortunately, standard methods used to obtain pore volume and size distribution (Barrett-Joyner-Halenda (BJH) approach via nitrogen adsorption or mercury porosimetry) cannot be applied to bio-aerogels. Bio-aerogels often possess large macropores (several hundreds of nanometers up to several microns). BJH method considers mainly mesopores and small macropores (below 200 nm), which makes only 10–20% of the total pore volume in bio-aerogels

(Robitzer, Di Renzo, & Quignard, 2011; Rudaz et al., 2014; Jiménez-Saelices, Seantier, Cathala, & Grohens, 2017; Groult & Budtova, 2018a). If mercury porosimetry is used, the change of bio-aerogel volume is often due to a compression and not mercury penetration in the pores (Rudaz, 2013; Rudaz et al. 2014). Imaging, such as SEM or 3D tomography, needs to "see" the mesopores and be able to analyse pores' complex shapes.

Till now, the mechanical properties of bio-aerogels have been tested under the uniaxial compression. Bio-aerogels can usually be compressed without breakage till 70-80% strain, in the majority of cases no shape recovery occurs. The linear window is very small, less than few per cent strain, and the compressive modulus is usually approximated by power-law of density.

Finally, thermal conductivity is often measured using either hot-wire or hot-plate methods and custom-made set-ups adapted for small samples. In the hot-wire method, a wire is placed between two disks of the material under investigation. The temperature is raised and measured at a certain distance from the wire as a function of time. The thermal conductivity is deduced from the temperature profile which is fitted by a known analytical dependence. In the hot-plate method the sample is placed between two plates; one of them is heated. The temperature of the other plate is recorded; temperature difference depends on the thermal conductivity of the material. In both methods, especially for materials with thermal conductivity comparable with that of air, the errors due to the "imperfections" in the set-up may become critical and lead to wrong results. Calibration with the known thermal superinsulating standard materials is a *sine qua non* condition for obtaining adequate results.

4. Case studies

4.1 Cellulose aerogels

255 Cellulose is the most abundant natural polymer that can be widely found in wood, plants, marine
256 animals and bacteria. Cellulose macromolecule is built of repeated *β*-1,4-linked anhydro-D-glucose
257 units, and the chains are organized in amorphous and crystalline sequences. The crystalline phase has
258 several polymorphs (cellulose I, II, III_I, III_{II}, IV_I, and IV_{II}) which reflect chains' packing; the most common
259 are cellulose I and II. Cellulose I corresponds to native cellulose with chains packed in the parallel
260 direction; this is determined by the biosynthesis. Cellulose II is produced by dissolving native cellulose
261 followed by coagulation (or regeneration) or by swelling native cellulose in a concentrated alkali and
262 then removing the swelling agent; the chains of cellulose II are packed in the anti-parallel direction
263 which is thermodynamically more stable. Till now only cellulose I and II have been used to make
264 aerogels.
265
266 **4.1.1 Cellulose I aerogels**
267 Nanocellulose (cellulose nanofibrils (CNF), bacterial cellulose (BC) and cellulose nanocrystals
268 (CNC)) is the most used cellulose type for making aerogels and foams. Excellent reviews on various
269 properties of porous nanocellulose materials have been published recently (Lavoine & Bergström 2017;
270 De France et al., 2017), and a recent review discusses nanocellulose materials for thermal applications
271 (Ahankari, Paliwal, Subhedar, & Kargarzadeh, 2021). Here we focus only on the works that report
272 thermal conductivity of nanocellulose-based aerogels. Nanocellulose was also mixed with other
273 substances; these materials will be called "composite aerogels". Porous materials with low thermal
274 conductivity, based on freeze-dried nanocellulose, neat or in composites, will also be considered.
275
276 **4.1.1.1 Neat cellulose I aerogels**

One of the first neat CNF aerogels with thermal conductivity below that of air were reported in 2014: CNFs were from surface carboxylated softwood bleached kraft pulp (pretreated with 2,2,6,6-tetramethylpiperidine-1-oxyl (TEMPO) as the catalyst) dispersed in dilute acid resulting in stiff free-standing hydrogels (Kobayashi, Saito, & Isogai, 2014). The density of aerogels obtained under supercritical drying was 0.01 – 0.02 g/m^3 and specific surface area around 500 – 600 m^2/g indicating a highly mesoporous material. The lowest value of thermal conductivity was around 0.018 W/(m·K) at aerogel density 0.017 g/cm^3 (Figure 4). The homogeneous morphology with pore sizes below 100 nm (as deduced from SEM, Figure 5a) shows that the obtained aerogel "fits" the characteristics of superinsulating materials, recall Section 2. Slightly higher conductivity, 0.022 W/(m·K) (the lowest value), was reported later by the same group, also for TEMPO-oxidized CNF aerogels (Sakai, Kobayashi, Saito, & Isogai, 2016); in this work thermal conductivity was calculated as a product of density, thermal diffusivity and specific heat capacity.

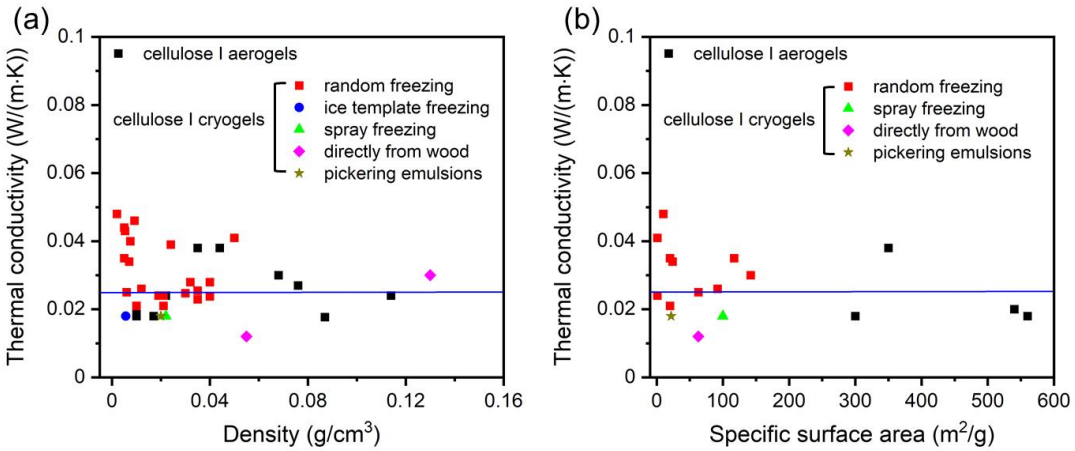

Figure 4.

Thermal conductivity of neat nanocellulose aero- and cryogels as a function of density (a) and specific surface area (b). Blue solid line corresponds to the thermal conductivity of air, 0.025 W/(m·K). Data

294 are taken from the following references: Fan, Chen, Yao, Sun, & jin, 2017; Ge et al., 2018; Guo L.,
295 Chen, Lyu, Fu, & Wang, 2018; Guo W. et al., 2018; Gupta, Verma, & Maji, 2018; Jiménez-Saelices et
296 al., 2017, Jiménez-Saelices et al., 2018; Kobayashi et al., 2014; Lazzari, Perondi, Zampieri, Zattera,
297 & Santana, 2019; Li et al., 2018; Munier, Apostolopoulou-Kalkavoura, Persson, Bergström, 2020;
298 Plappert, Nedelec, Rennhofer, Lichtenegger, & Liebner, 2017; Qi et al., 2019; Sakai, Kobayashi,
299 Saito, & Isogai, 2016; Seantier, Bendahou, Bendahou, Grohens, & Kaddami, 2016; Song et al., 2018;
300 Zhao, et al., 2015.
301
302 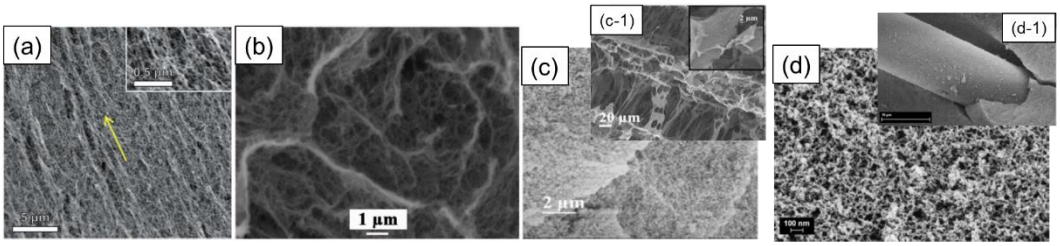

303 Figure 5.
304 SEM images of
305 (a) TEMPO-oxidized CNF aerogel, from Kobayashi, Y., Saito, T., & Isogai, A. (2014). Aerogels with
306 3D ordered nanofiber skeletons of liquid-crystalline nanocellulose derivatives as tough and
307 transparent insulators. Angewandte Chemie - International Edition, *53*, 10394–10397, reprinted with
308 permission from John Wiley and Sons
309 (b) spray freeze-dried TEMPO-oxidised CNF, reprinted from Carbohydrate Polymers, Vol 157,
310 Jiménez-Saelices, C., Seantier, B., Cathala, B., Grohens, Y., Spray freeze-dried nanofibrillated
311 cellulose aerogels with thermal superinsulating properties, Pages 105-113, Copyright 2017, with
312 permission from Elsevier,

(c) composite freeze-dried methyltrimethoxysilane functionalised CNF-hydrophobised silica aerogels (inset: (c-1) silylated CNF cryogels), from Zhao, S., Zhang, Z., Sèbe, G., Wu, R., Rivera Virtudazo, R. V., Tingaut, P., & Koebel, M. M. (2015). Multiscale assembly of superinsulating silica aerogels within silylated nanocellulosic scaffolds: Improved mechanical properties promoted by nanoscale chemical compatibilization. Advanced Functional Materials, *25*, 2326–2334, reprinted with permission from John Wiley and Sons;

(d) hydrophobic silica aerogel-like composite reinforced with man-made fibers Tencel® (inset: (d-1) Tencel® fiber within silica matrix), reprinted by permission from Springer, J Mater Sci 52:2210–2221, Ambient-dried thermal superinsulating monolithic silica-based aerogels with short cellulosic fibers, Markevicius, G., Ladj, R., Niemeyer, P., Budtova, T., & Rigacci, A, Copyright 2017

An original and intelligent approach for making superinsulating CNF aerogels was described in the work of Plappert et al: in order to decrease pore dimensions and reach Knudsen regime, low-density CNF aerogels were compressed (Plappert, Nedelec, Rennhofer, Lichtenegger, & Liebner, 2017). CNF was obtained by mechanically fibrillating periodate/chlorite pre-treated cellulose resulting in 2,3-dicarboxyl CNF. Aerogel compression to 20% of sample initial height allowed obtaining thermal conductivity of around 0.017 W/(m·K); the initial aerogel density was around 0.02 – 0.025 g/cm^3 and after compression 0.087 g/cm^3. This is a direct illustration of the importance of Knudsen effect and of the compromise between not too low density and not too large pore dimensions.

Freeze-drying still remains the main drying method used to make porous nanocellulose materials, most probably because lyophilization devices are much cheaper, easy to use and widely available opposite to high-pressure supercritical drying reactors. If using classical freeze-drying from water, pore

335 dimensions are usually from several microns to tens or even hundreds of microns as pores are the
336 replicas of ice crystals. Knudsen effect is not working in this case (see Section 2), and despite ultra-low
337 density, it is difficult to expect thermal conductivity below that of air. Various attempts were made to
338 decrease pores' dimensions. Jiménez-Saelices et al. reported that cryogels prepared by spray freeze
339 drying method possess larger fraction of mesopores (Figure 4b) as compared to the conventional
340 freeze-drying, with specific surface area of 80-100 m^2/g vs around 1 m^2/g, respectively (Jiménez-
341 Saelices, Seantier, Cathala, & Grohens, 2017). As a result, thermal conductivity of spray freeze-dried
342 CNF was around 0.018 -0.021 W/(m·K) vs 0.024-0.028 W/(m·K) for conventionally freeze-dried CNF,
343 the density of both types of materials was within the same interval. Jiménez-Saelices reported another
344 method to obtain thermal superinsulating CNF cryogels (Jiménez-Saelices, Seantier, Grohens, &
345 Capron 2018). They were made from freeze-dried Pickering emulsions stabilized with TEMPO-oxidized
346 CNF; cryogels with ultra-low density (0.012 – 0.03 g/cm^3), rather low specific surface area (15 – 65
347 m^2/g) and thermal conductivity 0.019 – 0.023 W/(m·K) were made. In this case a U-shaped conductivity-
348 density dependence was obtained, recall Figure 2. The authors hypothesized that so low thermal
349 conductivity of cryogels with not high surface area (thus not highly mesoporous) is due to closed
350 porosity which decreases radiative heat transfer.
351 Another way of decreasing the size of the pores was suggested by Seantier et al (Seantier,
352 Bendahou, Bendahou, Grohens, & Kaddami, 2016): the dispersed in water bleached cellulose fibers
353 were mixed with CNF or CNC made from the same source and the whole lyophilized. The added
354 nanocellulose was "filling the space" between cellulose macro-fibers leading to the decrease in thermal
355 conductivity from 0.028 (no nanocellulose) to 0.023 W/(m·K) (best value, 10-20% of CNF). Specific
356 surface area was within 110 – 160 m^2/g. A U-shape curves of conductivity vs density were obtained with

357 the lowest thermal conductivity at density around 0.03 - 0.04 g/cm^3 (see example in Figure S2).

358 Surprisingly, several studies report thermal conductivity below that of air even of highly macroporous
359 freeze-dried CNF. For example, the conductivity of CNF cryogels with specific surface area around 20
360 m^2/g was 0.019 – 0.021 W/(m·K) (the lowest values) which was even lower than those of aerogels
361 made from the same CNF with specific surface area around 300 – 350 m^2/g and having similar solid
362 volume fraction (Sakai et al., 2016). Chen et al. reported CNF-based cryogels with extremely low density,
363 0.005 g/cm^3, and thermal conductivity around 0.014 – 0.016 W/(m·K) (Chen et al., 2014). Specific
364 surface area was not reported, SEM images of some samples show pores of dimensions around 1 μm.

365 Varying the mode of freeze-drying, random or with the preferential direction of ice crystal growth
366 (see Figure S1), allows making nanocellulose cryogels with anisotropic thermal properties. For example,
367 CNF-based cryogel with anisotropic thermal conductivity was reported by Li et al. (2018). So-called
368 “nanowood” was made by the treatment of wood with NaOH and Na_2SO_3 heated to boiling temperatures,
369 followed by subsequent treatment with H_2O_2 to remove the lignin and most of the hemicellulose, and
370 freeze-dried. A material with density of 0.13 g/cm^3 and tubular structure was obtained, the diameter of
371 tubes was several tens of microns. Thermal conductivity in the radial direction was 0.032 W/(m·K) and
372 in the axial direction 0.056 W/(m·K). The same approach was reported by Song et al. (2018): the
373 conductivity of “nanowood” in the radial direction was 0.028 W/(m·K) and 0.12 W/(m·K) in the axial
374 direction.

375 The majority of nanocellulose-based cryogels, with pore size from few microns to several hundreds
376 of microns, have thermal conductivity higher than that of air, as expected (Figure 4). The conductivity
377 mainly depends on cryogel density. For example, Qi et al. (2019) made cryogels based on CNF from
378 cotton, poplar wood, bamboo and rice straw. At the same density, the samples had similar conductivity,

0.040 – 0.046 W/(m·K). For cotton-based CNF cryogels the conductivity decreased from around 0.049 to 0.028 W/(m·K) with increase the porosity from around 97.7% to 99.4%, respectively. The values of the thermal conductivity as a function of density and specific surface area of different nanocellulose cryogels are shown in Figure 4a,b.

4.1.1.2 Composite cellulose I aerogels

One of the ways to decrease the thermal conductivity of a porous material is to fill the pores with a material of conductivity below that of air but without a significant increase in the whole bulk density. Silica aerogels with the conductivity around 0.013 – 0.016 W/(m·K) are the best candidates for this purpose. It should also be taken into account that cellulose is hydrophilic and adsorbs water vapours. This increases thermal conductivity, as expected, and as demonstrated by Apostolopoulou-Kalkavoura et al : the conductivity of oven-dried foamed CNF increased from ~ 0.048 W/(m·K) to 0.085 W/(m·K) with relative humidity (RH) increase from 20 to 80 %, respectively (Apostolopoulou-Kalkavoura, Gordeyeva, Lavoine, Bergström, 2018). Surprisingly, the opposite trend was reported by the same group: thermal conductivity in the radial direction of unidirectionally freeze-dried CNF decreased with the increase of the relative humidity from 0.03 to 0.019 W/(m·K) for RH from 1 to 65 %, respectively, despite the increase in moisture uptake (Munier, Apostolopoulou-Kalkavoura, Persson, Bergström, 2020). The authors do not provide an explanation of this anomalous behavior. To avoid water vapours' adsorption, cellulose hydrophilization (often silylation) is performed. Below various composite aerogels based on nanocellulose mixed with other components and/or functionalized, are discussed.

A somewhat complex but efficient strategy to obtain thermal superinsulating composites was suggested by Zhao et al., 2015. CNF was hydrophobized with methyltrimethoxysilane (MTMS), freeze-

401 dried, filled with tetraethoxysilane (TEOS)-based sol, the latter also hydrophobized and the whole dried
402 with supercritical CO_2. While both non-hydrophobised and silylated CNF cryogels had very large
403 macropores (inset of Figure 5c), negligibly low specific surface area and thus thermal conductivity
404 above that of air (0.031 – 0.039 W/(m·K)), hydrophobic composites with silica aerogels in the pores of
405 CNF possessed conductivity 0.014 – 0.018 W/(m·K) (Zhao et al., 2015). Thanks to mesoporous silica
406 aerogel (Figure 5c), specific surface area of composite aerogels was high, 450 – 630 m^2/g. Higher was
407 the fraction of CNF, lower was the surface area and higher thermal conductivity. The mechanical
408 properties of composite aerogels under compression were improved as compared to the neat silica
409 aerogels. It should be noted that CNF and two dryings, lyophilization and supercritical, are not needed
410 to obtain strong hydrophobic silica aerogel-like materials with thermal superinsulation properties:
411 natural or man-made short cellulose fibers were dispersed in the prepolymerised TEOS, the latter
412 hydrophobized with hexamethyldisilazane and the whole dried at ambient pressure and 140 °C (Figure
413 5d) (Jaxel, Markevicius, Rigacci, & Budtova, 2017; Markevicius, Ladj, Niemeyer, Budtova, & Rigacci,
414 2017). The thermal conductivity of these composites was 0.016 – 0.018 W/(m·K), specific surface area
415 from 570 to 730 m^2/g, and mechanical properties under 3-point bending were significantly improved as
416 compared to silica aerogels.

417 Some composite cryogels based on CNF with thermal superinsulating properties were reported
418 despite very large macropores of the materials. For example, CNF/graphene oxide/zirconium
419 phosphate cryogels with low specific surface area (around 20 m^2/g), density 0.009 g/cm^3 and pores
420 with the size of several tens of microns were reported to possess thermal conductivity of around 0.018
421 W/(m·K) (Wang D. et al., 2020). Similar values were reported for CNF/graphene oxide/sepiolite
422 nanorods and CNF/graphene oxide/sepiolite nanorods/boric acid cryogels made via unidirectional ice-

templating (Figure S1) (Wicklein et al., 2015). The composites had tubular morphology with tubes' diameter of few tens of microns, and thermal conductivity in the radial direction was surprisingly low, 0.016 – 0.018 W/(m·K). The density was around 0.007 g/cm^3 and specific surface area was not reported. Lazzari et al. produced nanocellulose-biochar cryogels with density around 0.01 – 0.03 g/cm^3, high macroporosity as deduced from SEM (no specific surface area reported) and conductivity 0.021 – 0.026 W/(m·K) (Lazzari et al., 2019). Unfortunately, all these authors were not explaining how it was possible to overcome Knudsen effect.

Zhang X. et al. (2020) compared the influence of different freeze-drying methods (random freezing, unidirectional freezing, and bidirectional freezing) on the structure and thermal conductivity of polyimide/bacterial cellulose cryogels. Bidirectional freezing corresponds to a setup inducing two temperature gradients during freezing resulting in aligned lamellar structures. Cryogels prepared by random freezing had isotropic thermal conductivity 0.042 W/(m·K). Cryogels obtained with unidirectional freezing (tubular structure) possess thermal conductivity 0.037 W/(m·K) in the radial and 0.066 W/(m·K) in the axial directions. The thermal conductivity of bidirectional cryogels with lamellar morphology was 0.023 and 0.044 W/(m·K) in the radial and axial direction, respectively. The density of bidirectional cryogels was 0.05 – 0.1 g/cm^3, specific surface area was not reported; SEM images showed the distance between lamellas around 10 μm and pore walls of 1 to 2 μm. The authors interpret the lowest thermal conductivity of bidirectional cryogels in the radial direction as follows: "the parallel lamellar structure of b-PI/BC (here, bidirectional) aerogel would greatly reduce the heat transfer in the radial direction since the absence of interlamellar heat conduction" (Zhang X. et al., 2020).

The majority of nanocellulose-based composite cryogels reported in literature have low thermal conductivity but higher than that of air, as expected from material morphology with very large

445 macropores. A non-cellulose component is often used to increase hydrophobicity and/or improve fire
446 retardant properties by adding various substances, but these modifications usually increase the thermal
447 conductivity. For example, hydrophobised CNC-polyurethane cryogels possessed long-lasting
448 superhydrophobicity, anti-icing properties and oil absorbency efficiency, but conductivity was high,
449 0.075 W/(m·K) (Cai et al., 2020). Flame-retarding modification of CNF-based cryogels increased
450 thermal conductivity from 0.026-0.027 for neat CNF cryogel to 0.039 W/(m·K) for CNF-sepiolite (Gupta,
451 Verma, & Majie, 2019), to 0.032 W/(m·K) for CNF-N-methylol dimethylphosphonopropionamide/1,2,3,4-
452 butanetetracarboxylic acid (Guo L., Chen, Lyu, Fu, & Wang, 2018) and to 0.028 W/(m·K) for CNF-
453 sodium bicarbonate cryogels (Farooq, Sipponen, Sepplälä, & Österberg, 2018). Conductivity around
454 0.040 W/(m·K) were reported for CNF-hydroxyapatite (Guo W. et al. 2018) and CNF-aluminium based
455 metal organic frameworks cryogels (Zhou S. et al., 2020). The details on the conductivity and materials'
456 properties of various nanocellulose-based composite aerogels and cryogels are presented in Table 1.
457 As in the case of the reinforcement of silica aerogels with cellulose fibers and keeping thermal
458 superinsulating properties (Jaxel et al., 2017; Markevicius et al., 2017), nanocellulose is not a pre-
459 requisite for obtaining lightweight fire retardant and thermal insulating cellulose-based materials: for
460 example, wood fibers/palygorskite cryogels possess conductivity of 0.033 – 0.047 W/(m·K) at density
461 0.033 – 0.072 g/cm^3, respectively (Zhou X. et al., 2020)..

462 Table 1. Composite aerogels and cryogels involving cellulose I.

Material	Additional component	Density (g/cm^3)	Thermal conductivity (W/(m·K))	Specific surface area (m^2/g)	Young's modulus (MPa)	Water contact angle (°)	Drying method	Reference
CNF	nanozeolites		0.018	100	0.11	-	freeze-drying	Bendahou, Bendahou, Seantier, Grohens, & Kaddami, 2015
CNF	graphene oxide and sepiolite nanorods	0.0075	0.015	-	0.54	-	freeze-drying	Wicklein et al., 2015
	-	0.0056	0.018	-	0.08	-		
CNF	hydrophobized with MTMS	0.01-0.03	0.031-0.036	13-2	-	-	freeze-drying	Zhao et al., 2015
	without hydrophobized	0.007-0.018	0.034-0.039	24-9	-	-		
	neat CNF cryogels mixed with prepolymerised TEOS (polyethoxydisiloxane)	0.130-0.146	0.014-0.018	631-454	2.3-2.8	-	supercritical CO_2 drying	
	cryogels made from MTMS hydrophobized CNF mixed with PEDS-P75E20 (prepolymerized form of TEOS	0.128-0.133	0.018-0.020	756-675	1.8-1.3	-		

	containing a water-to-TEOS molar ratio of 1.5 and a SiO_2 content of 20% w/w in ethanol)							
CNF	-	0.055	-	11	5.93	-	ambient pressure drying	Fu et al., 2016
	tetraethylorthosilicate	0.059-0.295	0.023	14-700	5.42	-		
bleached cellulose fibers (palm tree)	-	0.04	0.028	-	0.013	-	freeze-drying	Seantier et al., 2016
	cellulose nanofibrils	0.04	0.023-0.028	161	0.062	-		
	cellulose nanocrystals	0.04	0.025-0.028	142	0.062	-		
CNF	-	0.002	0.048	10	-	-	freeze-drying	Fan et al., 2017
	AlOOH	0.0025	0.039	67	-	-		
Tencel fibers	Prepolymerised TEOS (polyethoxydisiloxane) hydrophobized with methyltrimethoxysilane (MTMS)	0.1-0.13	0.017-0.018	730-570	-	133-139	ambient pressure drying	Markevicius, Ladj, Niemeyer, Budtova, & Rigacci, 2017
		0.1-0.12	0.016-0.017	730-570	-	136-142	supercritical CO_2 drying	

CNF	triblock poly(ethylene glycol)-poly(propylene glycol)-poly (ethylene glycol) polyoxamer copolymer /Gluconic acid D-lactone/$CaCO_3$	0.012	0.043	-	-	-	freeze-drying	Apostolopoulou-Kalkavoura et al.,2018
CNF	sodium bicarbonate	-	0.028	-	-	-	freeze-drying	Farooq et al., 2018
Carboxymethyl cellulose	-	0.024	0.039	-	0.23	-	freeze-drying	Ge et al., 2018
	2D graphene oxide/boric acid	0.026	0.042	-	1.03	-		
CNF	-	0.006	0.025	63	0.002	-	freeze-drying	Guo L. et al., 2018
	1,2,3,4-butanetetracarboxylic acid/ N-methylol di-methylphosphonopropionamide	-	0.033	43	0.005	-		
CNF	-	0.050	0.041	1	0.17	-	freeze-drying	Guo W. et al., 2018
	hydroxyapatite	0.088	0.039	39	0.46	-		
CNF	-	0.012	0.026	180	-	-	freeze-drying	Gupta et al. , 2019
	sepiolite	0.024	0.035	341	-	-		
unbleached long fiber	-	0.01-0.019	0.021-0.024	-	-	-	freeze-drying	Lazzari, Perondi, Zampieri, Zattera, & Santana, 2019
	biochar	0.021-0.027	0.023-0.026	-	-	-		
CNF	-	0.006	0.025	12	0.04	-	unidirectional	Munier et al., 2020

	isotropic silica	0.019	0.021	94	0.15	-	freeze-drying	
	anisotropic silica	0.021	0.020	153	0.3	-		
CNF	-	0.004	0.049	10	0.08	-	freeze-drying	Wang D. et al., 2020
	hierarchical ZrP/RGO nanosheets	0.009	0.018	23	0.994	-		
bacterial cellulose	polyimide	0.046	0.042	-	-	-	freeze-drying	Zhang X. et al., 2020
			0.037 radial direction 0.06 axial direction	-	-	-	unidirectional freezing (ice templating)	
			0.023 radial direction 0.044 axial direction	-	-	-	bidirectional freeze-drying	
CNF	-	-	0.043	103	-	-	freeze-drying	Zhou S. et al., 2020
	metal–organic frameworks	-	0.041	227	-	-		

‘-’ without additional component or the data are not reported.

463

4.1.2 Cellulose II aerogels

Cellulose II aerogels, as well as other man-made cellulose materials, can be obtained via two main routes: either derivatization followed by cellulose regeneration or by dissolution in a direct solvent followed by coagulation (or precipitation). The former method has been used very rarely: cellulose aerogels were made from viscose (Ookuna et al., 1993) and from cellulose carbamate (Pinnow, Fink, Fanter, & Kunze, 2008). Thermal conductivity was not measured in these two cases. Various direct solvents have been used to make cellulose II aerogels (aqueous alkali, *N*-methylmorpholine-*N*-oxide monohydrate (NMMO), ionic liquids, zinc chloride ($ZnCl_2 \cdot 6H_2O$), calcium thiocyanate ($Ca(SCN)_2 \cdot 6H_2O$) and LiCl/*N,N*-dimethylacetamide (LiCl/DMAc)) with only one, 8% NaOH-water, used for gelation of cellulose solutions. The details on cellulose II aerogels preparation, properties and applications can be found in a recent review (Budtova, 2019).

4.1.2.1 Neat cellulose II aerogels

Thermal conductivity of neat cellulose II aerogels as a function of density and specific surface area is shown in Figure 6. The reader will notice much less experimental data on cellulose cryogels, as compared to nanocellulose-based cryogels (Figure 4). What is even more important is that opposite to nanocellulose aero- and cryogels, no value of thermal conductivity of neat cellulose II aero- and cryogels falls in the thermal superinsulation region.

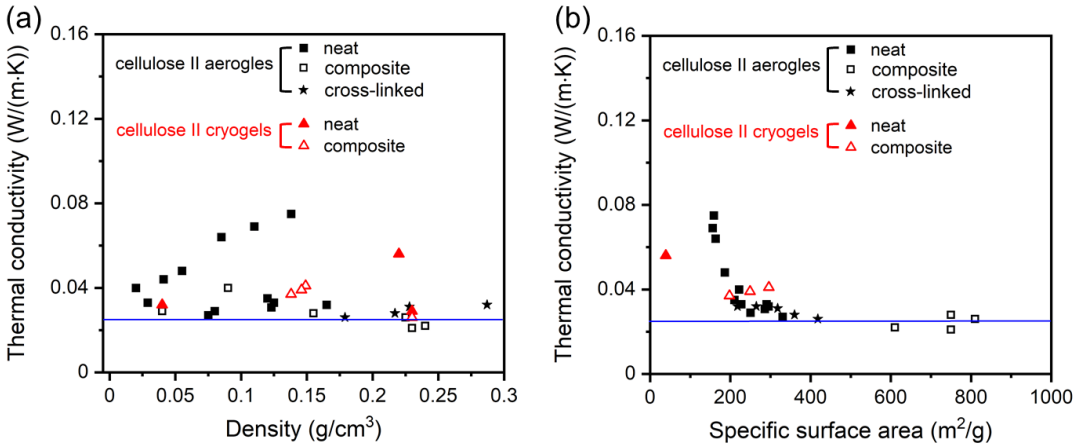

Figure 6

Thermal conductivity of neat (filled points) and composite (open points) cellulose II aerogels and cryogels as a function of density (a) and specific surface area (b). Blue solid line corresponds to the thermal conductivity of air. Data are taken from references: Demilecamps et al., 2015; Demilecamps, Alves, Rigacci, Reichenauer, & Budtova., 2016; Feng et al., 2016; Han, Zhang, Wu, & Lu, 2015; Laskowski, Milow, & Ratke, 2015; Mi, Ma, Yu, He, & Zhang, 2016; Rudaz, 2013; Karadagli et al., 2015; Shi, Lu, Guo, Sun, & Cao, 2013; Shi, Lu, Guo, Zhang, & Cao, 2013

Why cellulose II cryogels cannot be thermal superinsulating materials is clear from their morphology (Figure 7a): the density is low (0.01 – 0.2 g/cm^3) but the pores are large and the pore walls are thick and not porous. Specific surface area is rather low, from maximum 50 m^2/g for low molecular weight cellulose to maximum 130 m^2/g for high molecular weight cellulose (Buchtová & Budtova, 2016; Buchtová, Pradille, Bouvard, & Budtova, 2019).

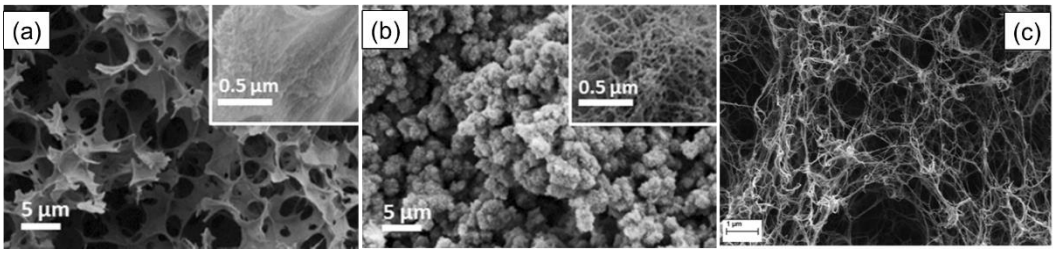

Figure 7

SEM images of cellulose II cryogel (a) and aerogel (b) both from microcrystalline cellulose dissolved in 1-ethyl-3-methylimidazolium acetate/DMSO and coagulated in ethanol, reprinted by permission from Springer, Cellulose, Cellulose aero-, cryo- and xerogels: towards understanding of morphology control, Buchtova N., Budtova T., Copyright 2016, and (c) aerogel from cellulose dissolved in $Ca(SCN)_2 \cdot 4H_2O$ and coagulated in ethanol, reprinted from J. of Supercritical Fluids, 106, Karadagli I., Schulz B., Schestakow M., Milow B., Gries T., Ratke L., Production of porous cellulose aerogel fibers by an extrusion process, 105-114., Copyright 2015, with permission from Elsevier

Cellulose II aerogels possess a finer fibrous morphology as compared to cryogels but seem to have too many large macropores (Figure 7b,c) and/or probably too thick pore walls, both being not favorable for thermal superinsulating properties (eq. 1). This is different from nanocellulose-based aerogels, compare aerogels' morphology shown in Figure 5a,b for nanocellulose-based aerogels and Figure 7 for cellulose II. In the view of decreasing pores' size and thus decreasing gaseous phase conductivity (eq. 3), cellulose was cross-linked with epichlorohydrin (ECH) in 8% NaOH-water (Rudaz, 2014). This allowed decreasing the conductivity from around 0.033 – 0.035 to 0.026 W/(m·K) (Figure 6). As mentioned in Section 3, unfortunately there is no suitable method to determine pore size distribution in bio-aerogels which is slowing down the understanding of their thermal conductivity properties.

As for the case of nanocellulose aerogels, efforts were made to decrease cellulose hydrophilicity expecting this would decrease thermal conductivity. This indeed helped but still the “barrier” of air conductivity was not overcome: thermal conductivity of tritylcellulose aerogels was 0.027 – 0.029 W/(m·K) (Demilecamps, Alves, Rigacci, Reichenauer, & Budtova, 2016), methyltrimethoxysilane (MTMS) treatment of cellulose cryogel decreased the conductivity from 0.032 to 0.029 W/(m·K) (Nguyen et al., 2014) and the same lowest value of conductivity, 0.029 W/(m·K), was obtained for cellulose cryogels treated with cold plasma (Shi, Lu, Guo, Sun, & Cao, 2013).

4.1.2.2 Composite cellulose II aerogels

In order to decrease gas phase conductivity in cellulose II aerogels, silica aerogels were used to replace air in the pores, as in the case of nanocellulose-based aerogels. To make an interpenetrated cellulose II-silica network turned out to be less evident than dispersing nanocellulose in silica sol. An attempt of using a common solvent of cellulose and sodium silicate, 8%NaOH-water, and one-pot approach, was tested; however, cellulose coagulated in the presence of silica and silica formed particles and not aerogels (Demilecamps, Reichenauer, Rigacci, Budtova, 2014). Mixing silica aerogel particles with cellulose dissolved in calcium thiocyanate slightly reduced the thermal conductivity as compared to neat cellulose aerogel but still remained high, 0.04 – 0.05 W/(m·K) (Laskowski, Milow, & Ratke, 2015).

Interpenetrated cellulose-silica networks with silica making aerogel phase in the pores of cellulose skeleton can be formed when impregnating coagulated cellulose (before drying) with silica sol followed by silica gelation and supercritical or freeze-drying. However, silica is very sensitive to pH and cellulose may be ionized after being dissolved in aqueous alkali; surface charges on the walls of the pores of cellulose network may perturb the formation of silica aerogels. This is what probably happened when

coagulated cellulose was impregnated with tetraethyl orthosilicate (TEOS): the conductivity surprisingly increased from 0.025 W/(m·K) for the neat cellulose aerogel to 0.04–0.05 W/(m·K) for composites (Cai et al., 2012). A possible reason could be high density of composite aerogel (0.3 – 0.6 g/cm^3) as compared to neat components (0.14 g/cm^3 and 0.19 g/cm^3 for cellulose and silica aerogels, respectively). A decrease of the thermal conductivity was reported for composite cellulose-silica aero/cryogels made via impregnation technique: from around 0.033 – 0.030 W/(m·K) for the neat cellulose aerogel or cryogel to 0.026 W/(m·K) for the composites (Shi, Lu, Guo, Zhang, & Cao., 2013).

It seems that the only one case known in literature when impregnation approach resulted in thermal conductivity of cellulose II-silica composite aerogel below that of air was when coagulated tritylcellulose network was impregnated with polyethoxydisiloxane, the latter gelled, silica hydrophobised and the whole dried with supercritical CO_2 (Demilecamps et al., 2016). Thermal conductivity was 0.021 – 0.022 W/(m·K) and SEM images confirm that silica phase completely fills the pores of cellulose matrix (Figure S3) (Demilecamps et al., 2016).

4.3 Chitin and chitosan aerogels

Chitin is the second most abundant natural polysaccharide. It is a linear polymer composed of (1→4)-β linked D-(N-acetyl)glucosamine. Chitin is similar to cellulose but with one hydroxyl group on each AGU replaced by an acetyl amine group. Chitin is organized in microfibrils embedded in proteins and associated with calcium salts. As for cellulose, aero- and cryogels based on chitin can be prepared either from various nanochitin forms, nanocrystals or nanofibers, or via polymer dissolution (Figure 3).

Very few publications report on the thermal conductivity of nanochitin aerogels: the lowest values were obtained for the neat nanochitin aerogel (0.027 W/(m·K)), silylation of this aerogel using chemical

562 vapor deposition increased the contact angle with water but also increased the conductivity to 0.030 –
563 0.036 W/(m·K) (Yan et al., 2020). Because of some difficulties in chitin dissolution, only few articles
564 describe the production of chitin aerogels and, to the best of our knowledge, none report their thermal
565 conductivity. As cellulose, chitin was shown to be soluble in imidazolium-based ionic liquids (Silva, Mano,
566 & Reis, 2017), which has not been explored yet for testing chitin aerogels' thermal conductivity.

567 Chitosan is a cationic polysaccharide obtained from chitin by decreasing the degree of acetylation
568 below 50 wt%. Replacing acetyl with amino group allows chitosan easy dissolution in acidic media such
569 as hydrochloric, dilute nitric, acetic, formic and lactic acids; the most commonly used solvent is 1%
570 acetic acid at pH around 4. Aerogels and cryogels can then be produced in the ways similar to cellulose
571 II.

572 The majority of chitosan aero- and cryogels that were tested for thermal insulation were made from
573 gels based on crosslinked chitosan, either with formaldehyde (Takeshita & Yoda, 2015), or with
574 glutaraldehyde (Zhu et al., 2020), or with ECH (Tang et al., 2019), or gelled in the presence of urea
575 (Guerrero-Alburquerque et al., 2020) (Figure 8). The lowest values of thermal conductivity of neat
576 chitosan aerogels were reported by Takeshita et al.: their aerogels were not only with thermal
577 superinsulating properties (0.022 W/(m·K)), but also with high specific surface area (545 m^2/g),
578 translucent and bendable (see aerogel morphology in Figure 9a) (Takeshita et al., 2015). Low values
579 of thermal conductivity of chitosan aerogels, around 0.024 – 0.025 W/(m·K), were obtained when
580 chitosan solutions were gelled in the presence of urea, but specific surface area was not high, 160 –
581 170 m^2/g (Guerrero-Alburquerque et al., 2020). The authors also explored drying the same gels at
582 ambient pressure, at ambient temperature and at 65 °C (Figure 9b, c). In both cases thermal
583 conductivity was significantly increased, from 0.036 to 0.068 W/(m·K) for the gels dried in ambient

conditions and from 0.031 to 0.056 W/(m·K) for those dried at higher temperature; interestingly, xerogels made at elevated temperature had higher specific surface area, 170-230 m^2/g, as compared to their aerogel counterparts (Guerrero-Alburquerque et al., 2020).

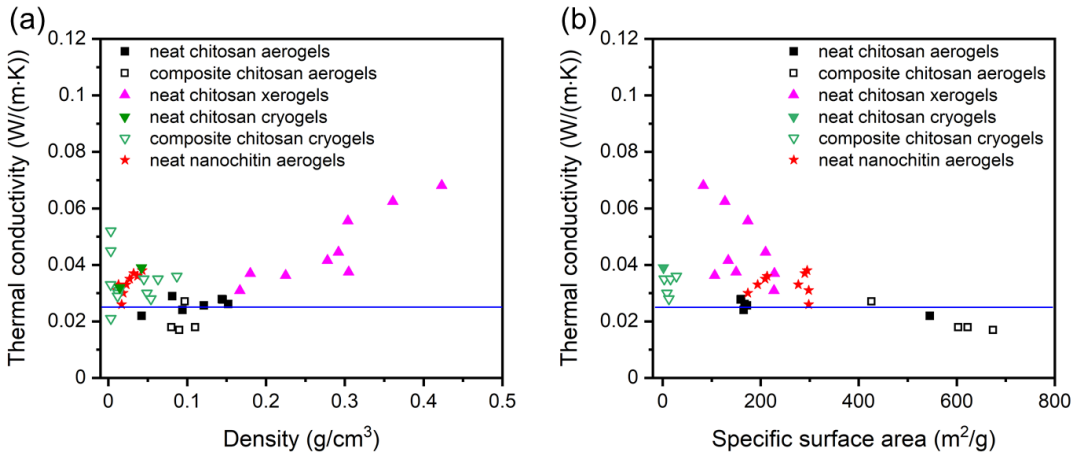

Figure 8.

Thermal conductivity of nanochitin and chitosan aero-, cryo- and xerogels as a function of density (a) and specific surface area (b). Blue solid line corresponds to the thermal conductivity of air. Data are taken from references: (Guerrero-Alburquerque et al., 2020; Takeshita et al., 2015; Wang et al., 2017; Zhang, Feng, Feng, Jiang, & Li, 2018; Zhao et al., 2016; Zhu et al., 2020; Tang et al., 2019; Yan et al., 2020)

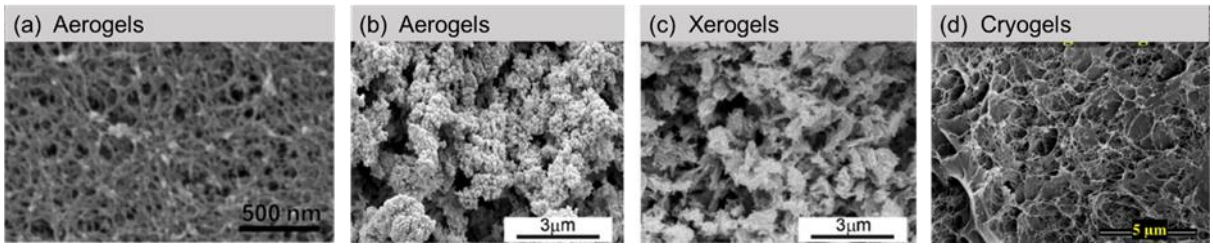

Figure 9

SEM images of chitosan aero-, cryo- and xerogels:

(a) formaldehyde-crosslinked chitosan aerogel, reprinted with permission from Takeshita, S., & Yoda, S. Chitosan Aerogels: Transparent, Flexible Thermal Insulators. Chemistry of Materials, *27*, 7569–7572. Copyright 2015 American Chemical Society;

(b) and (c) urea-crosslinked chitosan aerogel (b) and xerogel (c), reprinted with permission from Guerrero-Alburquerque, N., Zhao, S., Adilien, N., Koebel, M. M., Lattuada, M., & Malfait, W. J. Strong, Machinable, and Insulating Chitosan-Urea Aerogels: Toward Ambient Pressure Drying of Biopolymer Aerogel Monoliths. ACS Applied Materials and Interfaces, 12, 22037–22049. Copyright 2020 American Chemical Society;

(d) composite cryogels based on esterified cellulose nanocrystals/agar/chitosan, reprinted by permission from Springer Nature, Cellulose, Synthesis of light weight, high strength biomass-derived composite aerogels with low thermal conductivities, Tang, L., Zhuang, S., Hong, B., Cai, Z., Chen, Y., & Huang, B. 26, 8699–8712, Copyright 2019.

Composite chitosan aerogels were prepared either with organic or inorganic co-network. Chitosan-silica aerogels based on interpenetrated networks hydrophobized with hexamethyldisilazane were made by co-gelation of chitosan and sodium silicate: higher chitosan concentration increased aerogel density, improved compressive stress but slightly increased thermal conductivity from 0.0167 for the reference silica aerogel to 0.017 - 0.018 W/(m·K) (Zhao et al., 2016). Mixing chitosan with polyvinyl alcohol improved aerogel shape stability during processing and increased specific surface area from 308 to 426 m^2/g for the neat chitosan to composite chitosan-PVA aerogel, respectively; thermal conductivity of composite aerogel was 0.027 W/(m·K) (Zhang, Feng, Feng, Jiang, & Li, 2018).

Few publications report on the thermal conductivity of chitosan cryogels and its composites. Despite rather large pores (Figure 9d), the lowest thermal conductivity, 0.021 W/(m·K), was obtained for ECH-crosslinked chitosan/esterified cellulose nanocrystals/agar aerogels (Tang et al., 2019). Neat agar and chitosan/agar aerogels had much higher conductivity, 0.057 and 0.033 W/(m·K), respectively (Tang et al., 2019). Rather low conductivity was obtained for chitosan/NFC cryogels; it decreased from 0.032 for the neat chitosan aerogel to 0.029 W/(m·K) in the presence of NFC (Wang et al., 2017). Ice templating (recall Figure S1) was used to make anisotropic composites based on gluteraldehyde cross-linked chitosan/amino modified hydroxyapatite nanocrystals (HAP) (Zhu et al., 2020). Channels with rather flat pore walls were formed and specific surface area was low (from few m^2/g to few tens of m^2/g), similar to cellulose cryogels. Thermal conductivity in the radial direction first decreased from 0.039 to 0.028 W/(m·K) for the neat chitosan to composite chitosan cryogel, respectively, and increased to around 0.037 W/(m·K) with the increase of HAP concentration. On the opposite, in the axial direction the conductivity of composite cryogel was higher than that of the neat one (0.043 vs 0.039 W/(m·K), respectively (Zhu et al., 2020).

4.4 Pectin aerogels

Pectin is a ramified heteropolysaccharide usually extracted from citrus peel or apple pomace; it is widely used in food industry as a gelling and thickening agent. Pectin is a branched polymer with the main chain consisting of α-1,4-linked D-galacturonic acids which can be partly methylated or amidated at C6 position, or acetylated at O2 or O4 positions. Pectin degree of esterification (DE) defines the amount of methyl-esterified galacturonic acid resulting in high-methylated pectin (HM) with DE > 50% and low-methylated pectin (LM) with DE < 50%.

642 Opposite to cellulose and chitosan solutions, pectin solutions are “easy gelling”: esterified groups of
643 galacturonic acid are prone to hydrophobic interactions while non-esterified groups may interact via
644 hydrogen bonding if being in the protonated state or crosslink with polyvalent metal ions if deprotonated.
645 Depending on the intrinsic properties of pectin (chain length, branching, DE) and external conditions
646 (pH, temperature, ionic strength, presence of metal ions, sugars, etc.) pectin chains may associate in
647 different ways leading to the formation of various types of gels.

648 Pectin aerogels can be prepared either from gelled pectin solutions or by direct non-solvent induced
649 phase separation (Figure S4). The pathway of structure stabilization (or the state of the matter before
650 solvent exchange, gel or solution) is one of the key parameters influencing aerogel morphology and
651 density. When strong gels are formed via calcium-induced gelation at pH close pK_a, the aerogels are
652 with large pores, very low density (0.04–0.05 g/cm^3) and not very high specific surface area (around
653 250–350 m^2/g). When pectin network is formed via non-solvent induced phase separation from non-
654 gelled pectin solutions during solvent exchange step, the aerogels are mesoporous, with higher density
655 (0.12–0.15 g/cm^3) and high specific surface area (up to 600 m^2/g) (Groult & Budtova, 2018b).

656 Pectin aerogels turned out to be as performing thermal superinsulating materials as nanocellulose
657 aerogels, compare Figure 10 for pectin and Figure 4 for nanocellulose. The thermal conductivity of
658 pectin cryogels (Lu, Wu, & Chen, 2015) is much higher than that of aerogels, as expected (Figure 10).
659 A complete U-shape curve of thermal conductivity vs density was obtained for pectin aerogels (Figure
660 S5) (Groult et al., 2018a). Their density and morphology was varied by polymer concentration, gelation
661 conditions (hydrogel bonding or calcium crosslinking) and using non-solvent induced phase separation.
662 The lowest value of conductivity, around 0.015 W/m K, was obtained for aerogels made from non-gelled
663 pectin solutions, at pH 2 and pectin concentration of 2 wt%. Calcium-induced gelation results in LM

pectin aerogels of very low density (around 0.05 g/cm^3) but with too many macropores, thus reducing the contribution of Knudsen effect (Figure 11a, b).

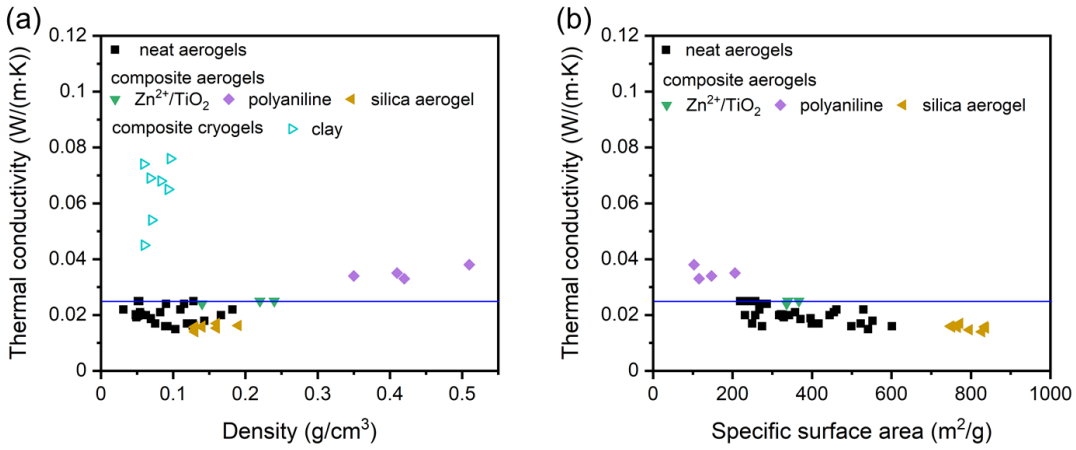

Figure 10.

Thermal conductivity of neat and composite pectin aerogels (filled points) and cryogels (open points) as a function of density (a) and specific surface area (b). Blue solid line corresponds to the thermal conductivity of air. Data taken from references: Groult et al., 2018a; Lu, Wu, & Chen, 2015; Nešić et al., 2018; Rudaz et al., 2014; Zhao, Chen, & Chen, 2017; Zhao et al., 2015.

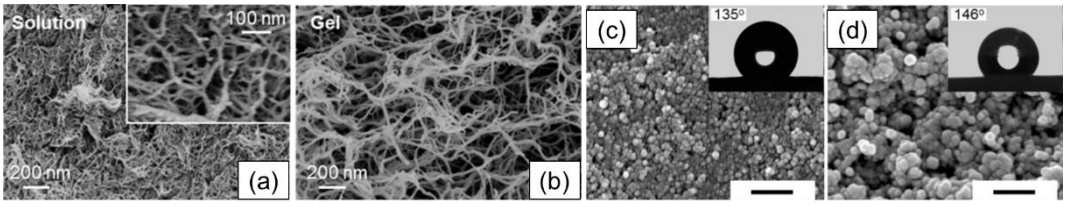

Figure 11

SEM images of

(a) neat pectin aerogels made from dissolved 3 wt% not cross-linked LM pectin at pH 2,

(b) the same but cross-linked with calcium, reprinted from Carbohydrate Polymers, Vol 196, Groult, S. & Budtova, T. Thermal conductivity/structure correlations in thermal superinsulating pectin aerogels, Pages 73-81, Copyright 2018, with permission from Elsevier;
(c) hydrophobized HM pectin-silica composite aerogels made from the mixtures at pH 1.5 and (d) the same at pH 3, the insets in (c) and (d) show the water contact angle. Reprinted with permission from John Wiley and Sons, Zhao, S., Malfait, W. J., Demilecamps, A., Zhang, Y., Brunner, S., Huber, L., Tingaut, P., Rigacci, A., Budtova, T., & Koebel, M. M. (2015). Strong, Thermally Superinsulating Biopolymer-Silica Aerogel Hybrids by Cogelation of Silicic Acid with Pectin. Angewandte Chemie - International Edition, 54, 14282–14286.

Very low thermal conductivity, 0.014 – 0.017 W/(m·K) (Figure 10), was also obtained for HM pectin-silica composite aerogels hydrophobized with hexamethyldisilazane (Zhao et al., 2015). By varying pectin:sodium silicate ratio in the mixture and tuning gelation conditions by pH, homogenous mesoporous and “neck-free” composite aerogels were prepared (Figure 11c, d). Specific surface area of these composite aerogels was very high due to silica aerogel phase. Other pectin-based composite aerogels with low thermal conductivity (0.022-0.025 W/(m·K)) were made by mixing LM amidated pectin with TiO_2 and Zn^{2+}; aerogels possessed antibacterial properties but the conductivity increased in the presence of TiO_2 (Nešić et al., 2018). When LM pectin was mixed with polyaniline, the composite aerogels were of thermal conductivity 0.033-0.038 W/(m·K) and showed flame retardant property (Zhao, Chen, & Chen, 2017). These higher values can be explained by high density of aerogels, 0.41 – 0.51 g/cm^3 and rather low specific surface area, 100 – 205 m^2/g, indicating low mesoporosity (Zhao, Chen, & Chen, 2017).

700 **4.5 Starch aerogels**

701 Starch is composed of amylose, a linear (1→4)-α linked glucan, and amylopectin, a (1→4)-α-linked
702 D-glucose with (1 → 6)-α branches. There are two main ways of starch processing: via
703 thermomechanical treatment and via dissolution. The first one leads to starch melting; it can then be
704 processed as a thermoplastic polymer. This processing route can be used to obtain starch foams but
705 not aerogels. The second one is gelatinization: heating starch granule suspension in water resulting in
706 granule swelling, loss of crystallinity, amylose leaching out and granule burst. Gelatinization is a
707 complex process not always leading to full starch dissolution: after granules' burst, a colloidal
708 suspension consisting of granule remnants and polysaccharides in solution is formed. The amount,
709 integrity and size of granules' remnants depend on several factors such as pasting temperature; for
710 example, melting temperature of amylose-based double helices, which stabilize granules' ghosts, is
711 above 130 °C. Another factor influencing dissolution is the presence of proteins/lipids which form a skin
712 and prevent granule swelling. If willing to obtain starch aerogels with specific surface area as high as
713 possible, starch needs to be well dissolved as granules and their remnants are non-porous. The
714 influence of non-dissolved entities has been reported for cellulose aerogels: the former decrease
715 cellulose aerogel specific surface area and increase the density (Korhonen & Budtova, 2020), both
716 trends being not favourable for reaching low thermal conductivity.

717 Most of starch solutions are gelling upon temperature decrease which is known as retrogradation
718 process. Numerous parameters affect starch aerogel properties and morphology: starch type and
719 concentration, retrogradation conditions and type of non-solvent (Druel, Bardl, Vorwerg, & Budtova,
720 2017; García-González, Uy, Alnaief, & Smirnova 2012; Glenn & Irving, 1995; Ubeyitogullari & Ciftci,
721 2016; Zou & Budtova, 2020). Till now, very few works report on the thermal conductivity of starch

aerogels and even less provide both the density and specific surface area (Figure 12a,b). The first authors who reported the low conductivity of starch aerogels (they were called “microcellular foams”), 0.024-0.036 W/(m·K), were Glenn & Irving (1995). Next, Druel et al. reported the influence of starch type and retrogradation time on the thermal conductivity of starch aerogels (Druel et al., 2017). Pea starch aerogels possess the lowest thermal conductivity (0.021-0.023 W/(m·K)) compared to waxy potato starch, regular potato starch and high amylose corn starch due to the lowest density and finest morphology (Figure 12c,d).

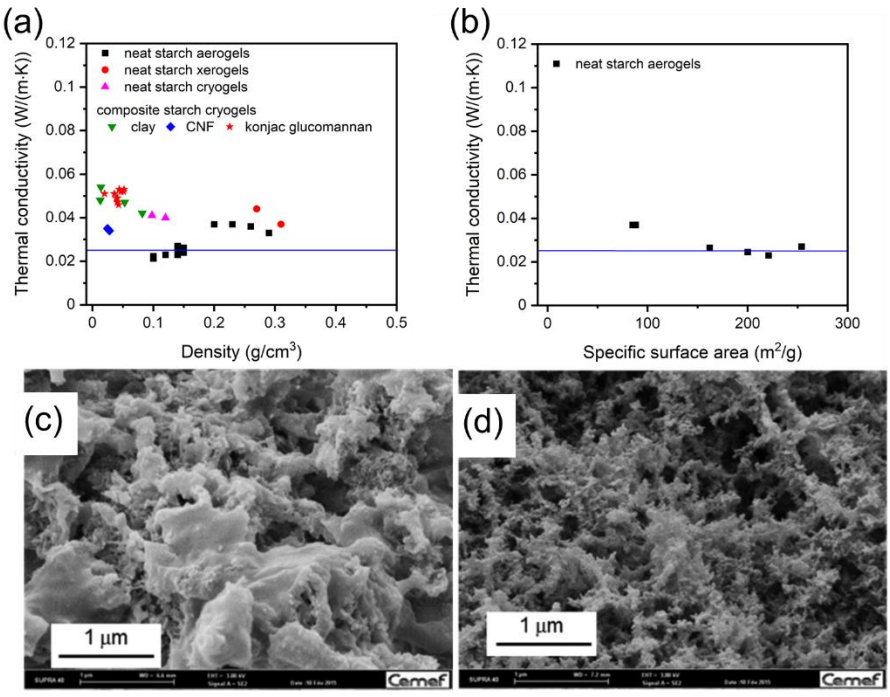

Figure12.

(a) and (b): thermal conductivity of starch porous materials as a function of density and specific surface area, respectively. Blue solid line corresponds to the thermal conductivity of air. Data are taken from Druel et al., 2017; Glenn et al., 1995; Wang et al., 2018; Ye et al., 2019; Yildirim, Shaler, Gardner, Rice, & Bousfield, 2014.

(c) and (d): SEM images of regular potato (c) and pea (d) starch aerogels with thermal conductivity 0.037 and 0.023 W/(m·K), respectively. Reprinted with permission from Druel, L., Bardl, R., Vorwerg, W., & Budtova, T. Starch Aerogels: A Member of the Family of Thermal Superinsulating Materials. Biomacromolecules, 18, 4232–4239. Copyright 2017 American Chemical Society.

The thermal conductivity of neat and composite starch cryogels is much higher (0.040-0.060 W/(m·K)) than that of aerogels due to very large macropores formed during freezing process (Wang et al., 2018; Ye et al., 2019; Yildirim, Shaler, Gardner, Rice, & Bousfield, 2014).

4.6 Alginate aerogels

Alginate is a linear polyuronic acid composed of β-D-mannuronic acid and α-L-guluronic acid in various proportions. Their ratio practically does not vary within algae specie but may vary between 0.45 and 1.85 among different algae sources. As pectin, it is an “easy gelling” polysaccharide, and aerogels can be prepared either from alginate solutions gelled with polyvalent metal ions (Gurikov, Raman, Weinrich, Fricke, & Smirnova, 2015; Raman, Gurikov, & Smirnova, 2015) or via non-solvent induced phase separation (Tkalec, Knez, & Novak, 2015). Alginate aerogels have been extensively studied as drug delivery systems, but only few publications report their thermal conductivity (Figure 13). This is surprising as alginate aerogels are known to have low density and high specific surface area, both favourable for low thermal conductivity.

Some alginate aerogels and their composites have been reported as thermal superinsulating materials with conductivity around 0.018-0.022 W/(m·K) (Gurikov et al., 2015; Raman et al. 2015), their specific surface area was 370 – 670 m^2/g and 210 – 810 m^2/g, respectively. Tkalec et al. reported high

conductivity (for aerogels), 0.08 W/(m·K), but specific surface area was only 150 m^2/g (Tkalec et al., 2015). When alginate was gelled within PET nonwoven, the thermal conductivity of the composite aerogel was 0.039 W/(m·K) and specific surface area was surprisingly very low, only 18 m^2/g (Ahmad Ulker, & Erkey, 2018)). Alginate cryogels have higher thermal conductivity, 0.035-0.047 W/(m·K), as compared to alginate-based aerogels, and as expected from cryogel morphology and low specific surface area.

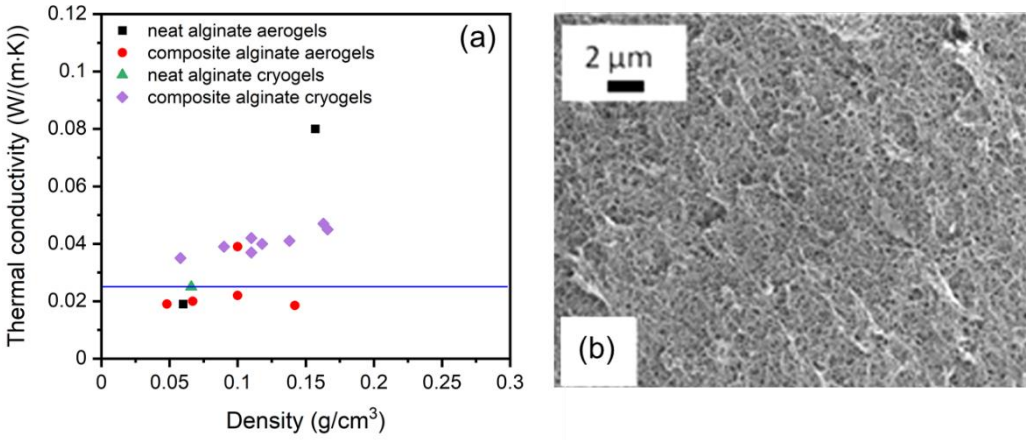

Figure13.

(a) Thermal conductivity of alginate aerogels and cryogels as a function of density. Blue solid line corresponds to the thermal conductivity of air. Data are taken from the references Gurikov et al., 2015; Li, He, Qin, Chen, & Chen, 2019; Raman et al., 2015; Shang et al., 2016; Tkalec et al., 2015; Ahmad et al., 2018;

(b) SEM image of composite alginate-lignin aerogels, reprinted from J. of Supercritical Fluids, 106, S.P. Raman, P. Gurikov, I. Smirnova, Hybrid alginate based aerogels by carbon dioxide induced gelation:Novel technique for multiple applications, Pages 23-33, Copyright 2015, with permission from Elsevier.

776

777 **4.7 Non-polysaccharide bio-aerogels**

778 Bio-aerogels can be made from natural polymers such as proteins. For example, silk fibroin aerogels
779 with density 0.02 g/cm^3, specific surface area 412 m^2/g and thermal conductivity 0.026 W/(m·K) were
780 reported (Maleki, Montes, Hayati-Roodbari, Putz, & Huesing, 2018; Maleki, Whitmore, & Hüsing, 2018).
781 In the view of improving aerogel mechanical properties, silk fibroin was mixed with organosilanes
782 (tetramethylorthosilicate and 5-(trimethoxysilyl)pentanoic acid or polymethylsilsesquioxane and 5-
783 (trimethoxysilyl)pentanoic acid) in the presence of surfactant, byproducts extracted by solvent
784 exchange with methanol and aerogels were made from such interpenetrated networks. Density and
785 specific surface area increased as compared to the neat silk fibroin aerogels, but, unfortunately, thermal
786 conductivity also increased to 0.033 – 0.043 W/(m·K) (Maleki et al., 2018; Maleki et al., 2018). Silk
787 fibroin is a very interesting but expensive matter with rather complex extraction and purification
788 procedure; its aerogels can probably have potential in biomedical applications. Some other proteins
789 have been used to make aerogels but their thermal conductivity was not reported.

790 Finally, amino acid-based (phenylalanine and leucine, dissolved in toluene or tetralin) hydrophobic
791 supramolecular aerogels were reported (Jamart-Grégoire et al., 2016). The density was very low,
792 0.004–0.03 g/cm^3 and the specific surface area around 90 m^2/g. These aerogels possessed thermal
793 conductivity of 0.026–0.027 W/(m·K).

794

795 **5. Discussion: overview, problems and prospects**

796 The results presented above show that some bio-aerogels are thermal superinsulating materials,
797 with conductivity comparable to that of superinsulating silica aerogels. This is a very promising result.

798 Except for nanocellulose based aerogels and cryogels, for which data are very scattered, the general
799 trend for bio-aerogels shows that in order to have the lowest possible thermal conductivity, the density
800 should be around 0.1 g/cm^3 and specific surface area above several hundreds of m^2/g. High specific
801 surface area can be seen as a prerequisite to have Knudsen effect, as demonstrated for aerogels based
802 on cellulose II composites, chitosan, pectin, starch and alginate. In other words, in addition to high
803 porosity, pore sizes should be below the mean free path of air molecule, recall Section 2 and Figure 2.
804 This is in the agreement with previously reported trends for inorganic and synthetic polymer aerogels.
805 One of the most intriguing questions is why it is not possible (at least never reported) to make thermal
806 superinsulating cellulose II neat aerogels while this is feasible for cellulose I counterparts and other bio-
807 aerogels? During coagulation cellulose chains are packing in a thermodynamically stable antiparallel
808 direction stabilized by intra- and intermolecular hydrogen bonds. Is this the reason of the “unfavourable”
809 morphology with rather large pores and/or thick pore walls? Molecular modelling of structure formation
810 during coagulation could help a better understanding of thermal conductivity properties of cellulose-
811 based aerogels. Here supercritical drying could be a way to visualize the morphology as a function of
812 processing conditions, e.g. polymer concentration and type of solvent and non-solvent. It should be
813 noted that such important parameter as cellulose crystallinity was never considered when analyzing
814 thermal conductivity. Modelling of thermal conductivity of bio-aerogels is totally absent, which makes
815 this area developing according to trials and errors approach.
816 If willing to use a material for thermal insulation, several important characteristics need to be
817 considered. One is the price of the starting matter. We will not make here a technico-economical
818 evaluation of the production of bio-aerogels; it is a topic of a separate study which should be
819 accompanied by life cycle analysis. However, it should be noted that polysaccharides described above

820 used to make bio-aerogels are natural, renewable and not expensive.

821 The mechanical properties are the key parameter to consider if willing to use a material for thermal
822 insulation. The majority of literature on polysaccharide-based aerogels study their mechanical
823 properties under the uniaxial unconfined compression, most probably because of the easiness in the
824 preparation and handling of cylindrical samples. The results from bio-aerogels' 3-point bending test,
825 which would be very useful for practical applications, are strongly missing. All literature on bio-aerogels
826 agrees that under the uniaxial compression, a typical stress-strain curve is similar to that of foams
827 (Gibson & Ashbi, 1999) with a small linear region (few % strain and less) followed by a stress plateau
828 corresponding to progressive cell walls buckling and collapse, and densification region (see, for
829 example, Rudaz et al., 2014; Kobayashi et al., 2014; Druel, Bardl, Vorwerg, & Budtova, 2017; Plappert
830 et al., 2017; Plappert et al., 2018; Rennhofer et al., 2019; Buchtová, Pradille, Bouvard, & Budtova 2019).
831 Bio-aerogels, including those that are thermal superinsulating, are not breaking under compression,
832 with strain at densification reaching 70-80% (Kobayashi, Saito, & Isogai, 2014; Rudaz et al., 2014;
833 Plappert, Nedelec, Rennhofer, Lichtenegger, & Liebner, 2017). This is a very important factor in favour
834 of using bio-aerogels for thermal insulation applications. Silica aerogels are known to be brittle, and
835 thus various reinforcement strategies are used. They involve either short or long fibers (inorganic,
836 synthetic polymer or cellulose-based) (Bardy, Mollendorf, & Pendergast, 2007; Jaxel et al. 2017) with
837 the classical example being so-called aerogel "blankets". Another option to reinforce silica aerogels is
838 to use modified precursors and/or cross-linking (G. Zhang et al., 2004; Hayase et al., 2014; Hayase,
839 Kanamori, Maeno, Kaji, & Nakanishi, 2016). Such modifications are not required for bio-aerogels.

840 Depending on bio-aerogel density, the compressive modulus varies from hundreds KPa to tens MPa.
841 As for organic and inorganic aerogels, compressive modulus is power law dependent on bio-aerogel

842 bulk density with exponent varying from 3 to 4. The majority of literature reports zero Poisson ratio for
843 bio-aerogels, however, recently it was demonstrated that Poisson ratio of low-density cellulose II
844 aerogels is around 0.15 – 0.20, as for silica aerogels (Gross, Reichenauer, & Fricke, 1988), and it
845 decreases with bio-aerogel density increase (Buchtová et al., 2019).

846 There are two strong disadvantageous properties of bio-aerogels that may explain why they are still
847 not considered for a large-scale thermal insulation application. One is drying in supercritical conditions.
848 Despite that supercritical CO_2 is used in various industrial sectors (for separation and extraction, in
849 polymer processing for plasticization and foaming, in chemical and biochemical reactions, for drying
850 samples for scanning electron microscopy), supercritical drying involves high-pressure technology and
851 it is a batch process. To obtain bio-based porous materials with the thermal conductivity and mechanical
852 properties equivalent to those of bio-aerogels but avoiding drying in supercritical conditions is a
853 challenging task which till now is not solved.

854 If drying polysaccharide gels at ambient pressure or in vacuum, pores are closing due to capillary
855 pressure (eq. 5) and remain closed as chains collapse and also due to strong hydrogen bonds that may
856 be formed between numerous hydroxyl groups. To avoid pore closing and network strong densification,
857 various procedures were suggested: for example, a multi-step liquid exchange procedure replacing
858 water with less polar liquids (Svensson, Larsson, Salazar-Alvarez, & Wågberg, 2013), surface
859 esterification which was applied on nanofibrillated cellulose to obtain hydrophobic porous nanopaper
860 (Sehaqui, Zimmermann, & Tingaut, 2014), foaming (Cervin et al., 2013) and etherification of cellulose
861 with hydrophobic moieties in homogeneous conditions (Pour, Beauger, Rigacci, & Budtova, 2015). In
862 all cases mentioned above thermal conductivity was not reported but specific surface area was not high
863 suggesting low mesoporosity and thus limited input of Knudsen effect.

One option to solve the problem of irreversible mesopores' closure might be performing surface functionalization of a polysaccharide gel pore walls before drying in the same way as it is done for silica gels. To make aerogel-like material from ambient pressure dried alkoxide- or sodium silicate gels, their pore walls are grafted with $Si(CH_3)_3$ groups using hexamethyldisilazane (HMDZ), trimethylchlorosilane (TMCS) or hexamethyldisiloxane (HMDS) (see, for example, Schwertfeger et al., (1998)). This leads to the so-called ‘‘spring-back effect,’’ i.e. re-opening of the pores at the final stage of drying due to the repulsion of the grafted groups (see, for example, Hayase et al. (2016)). However, due to the inherent brittleness of the silica network which is built of nanometer-size particles organized in a “pearl necklace”, the initially monolithic gel breaks into sub-centimeter size pieces. These pieces possess aerogel properties, i.e. are of low density, mesoporous and their packed bed can be of very low thermal conductivity, around 0.017 W/(m·K) (Koebel, Huber, Zhao, & Malfait, 2016). The advantage of such silylation is that it also makes the functionalised silica hydrophobic resisting aging.

The second disadvantage is bio-aerogel aging which occurs due to the adsorption of water vapours by naturally hydrophilic polysaccharides. This is especially pronounced for bio-aerogels based on water-soluble polysaccharides. As mentioned above for the case on CNF foams, a two-fold increase of the thermal conductivity was recorded for the relative humidity increasing from 20 to 80 RH% (Apostolopoulou-Kalkavoura et al., 2018). A similar result was obtained for cellulose II cryogels (Shi, Lu, Guo, Sun, & Cao, 2013). When the latter were cold-plasma hydrophobized, the thermal conductivity remained around 0.030 – 0.035 W/(m·K) but did not vary as a function of humidity. To the best of our knowledge, the aging of bio-aerogels, i.e. the evolution of density, specific surface area, thermal conductivity and mechanical properties, is practically not studied. Till now, no strategy is developed to “save” thermal superinsulation properties of bio-aerogels. As for silica aerogels, pore surface

functionalization of polysaccharide gels could, potentially, help the preservation of network structure against collapse during drying at ambient pressure and decrease water vapours adsorption. However, harsh chemistry should be avoided.

6. Conclusions

This review presents the current status on thermal conductivity of bio-aerogels and some other porous polysaccharides, in the view of their potential use for thermal insulation. A special attention is paid on the possibility of reaching the conductivity below that of air, i.e. thermal superinsulation region. The influence of polymer source and processing conditions on the thermal conductivity is analysed via material density and specific surface area. The latter is used to judge on the mesoporosity of the material and thus on the applicability of Knudsen effect.

Within the well selected preparation conditions, all bio-aerogels made up to now – based on nanocellulose, pectin, alginate, starch and chitosan – can possess conductivity in thermal superinsulating region, except cellulose II aerogels. Why it is not possible to obtain thermal superinsulating cellulose II aerogels remains an open question. Modelling of structure formation upon coagulation of polysaccharides and of bio-aerogels' thermal conductivity could help better tuning their properties.

The opportunities and challenges of bio-aerogels in the view of their use for thermal insulation are discussed. Bio-aerogels have attractive mechanical properties, but they are aging and supercritical drying should be replaced by ambient pressure drying provided the properties of aerogels are preserved. Solving these problems involves interesting and in-depth fundamental research. A technico-economical

907 evaluation of bio-aerogels' production is also needed. There is thus still a lot of exciting research to do

908 for making high performance thermal insulating bio-based materials.

References

Aerogels Handbook (2011), in Advances in Sol-Gel Derived Materials and Technologies, Eds. M. A. Aegerter, M. Prassas, Springer Science and Business Media LLC: Berlin/Heidelberg, Germany.

Ahankari, S., Paliwal, P., Subhedar, A., & Kargarzadeh, H. (2021). Recent Developments in Nanocellulose-Based Aerogels in Thermal Applications: A Review. *ACS Nano*, 15, 3849−3874.

Ahmad, F., Ulker, Z., & Erkey, C. (2018). A novel composite of alginate aerogel with PET nonwoven with enhanced thermal resistance. *Journal of Non-Crystalline Solids*, *491*, 7–13.

Alam M. , Singh H., & Limbachiya. M. C. (2011). Vacuum Insulation Panels (VIPs) for building construction industry - A review of the contemporary developments and future directions. *Applied Energy*, *11*, 3592–3602.

Apostolopoulou-Kalkavoura, V., Gordeyeva, K., Lavoine, N., & Bergström, L. (2018). Thermal conductivity of hygroscopic foams based on cellulose nanofibrils and a nonionic polyoxamer. *Cellulose*, *25*, 1117–1126.

Bardy, E. R., Mollendorf, J. C., & Pendergast, D. R. (2007). Thermal conductivity and compressive strain of aerogel insulation blankets under applied hydrostatic pressure. *Journal of Heat Transfer*, *129*, 232–235.

Bendahou, D., Bendahou, A., Seantier, B., Grohens, Y., & Kaddami, H. (2015). Nano-fibrillated cellulose-zeolites based new hybrid composites aerogels with super thermal insulating properties. *Industrial Crops and Products*, *65*, 374–382.

Buchtová, N., & Budtova, T. (2016). Cellulose aero-, cryo- and xerogels: towards understanding of morphology control. *Cellulose*, *23*, 2585–2595.

Buchtová, N., Pradille, C., Bouvard, J. L., & Budtova, T. (2019). Mechanical properties of cellulose

931 aerogels and cryogels. *Soft Matter*, *15*, 7901–7908.

932 Budtova, T. (2019). Cellulose II aerogels: a review. *Cellulose, 26*, 81-121.

933 Budtova, T., Aguilera, D. A., Beluns, S., Berglund, L., Chartier, C., Espinosa, E., Gaidukovs, S., Klimek-

934 kopyra, A., Kmita, A., Lachowicz, D., Liebner, F., Platnieks, O., Rodríguez, A., Navarro, L. K. T.,

935 Zou, F., & Buwalda, S. J. (2020). Biorefinery approach for aerogels. *Polymers*, *12*, 1–63.

936 Cai, C., Wei, Z., Huang, Y., Ding, C., Wang, P., Song, J., Deng, L., Fu, Y., & Zhong, W. H. (2020).

937 Ultralight Programmable Bioinspired Aerogels with an Integrated Multifunctional Surface for Self-

938 Cleaning, Oil Absorption, and Thermal Insulation via Coassembly. *ACS Applied Materials and*

939 *Interfaces, 12*, 11273-11286.

940 Cai, J., Liu, S., Feng, J., Kimura, S., Wada, M., Kuga, S., & Zhang, L. (2012). Cellulose-silica

941 nanocomposite aerogels by in-situ formation of silica in cellulose gel. *Angewandte Chemie -*

942 *International Edition*, *51*, 2076–2079.

943 Cervin, N. T., Andersson, L., Ng, J. B. S., Olin, P., Bergström, L., & Waìšgberg, L. (2013). Lightweight

944 and strong cellulose materials made from aqueous foams stabilized by nanofibrillated cellulose.

945 Biomacromolecules, 14(2), 503–511.

946 Chen, W., Li, Q., Wang, Y., Yi, X., Zeng, J., Yu, H., Liu, Y., & Li, J. (2014). Comparative study of aerogels

947 obtained from differently prepared nanocellulose fibers. *ChemSusChem*, *7*, 154–161.

948 De France, K. J., Hoare, T., & Cranston, E. D. (2017). Review of Hydrogels and Aerogels Containing

949 Nanocellulose. *Chemistry of Materials*, *29*, 4609–4631.

950 Demilecamps, A., Alves, M., Rigacci, A., Reichenauer, G., & Budtova, T. (2016). Nanostructured

951 interpenetrated organic-inorganic aerogels with thermal superinsulating properties. *Journal of*

952 *Non-Crystalline Solids*, *452*, 259–265.

Demilecamps, A., Beauger, C., Hildenbrand, C., Rigacci, A., & Budtova, T. (2015). Cellulose-silica aerogels. *Carbohydrate Polymers*, *122*, 293–300.

Demilecamps, A., Reichenauer, G., Rigacci, A., & Budtova, T. (2014). Cellulose-silica composite aerogels from “one-pot” synthesis. *Cellulose*, *21*, 2625–2636.

Druel, L., Bardl, R., Vorwerg, W., & Budtova, T. (2017). Starch Aerogels: A Member of the Family of Thermal Superinsulating Materials. *Biomacromolecules*, *18*, 4232–4239.

Ebert, H.P. (2011). Thermal Properties of Aerogels, in Aerogels Handbook (Advances in Sol-Gel Derived Materials and Technologies). M. A. Aegerter, N. Leventis, & M. M. Koebel (Eds.). New York Dordrecht Heidelberg London: Springer Science and Business Media, p. 537

Fan, B., Chen, S., Yao, Q., Sun, Q., & Jin, C. (2017). Fabrication of cellulose nanofiber/AlOOH aerogel for flame retardant and thermal insulation. *Materials*, *10*, 1–10.

Farooq, M., Sipponen, M. H., Seppälä, A., & Österberg, M. (2018). Eco-friendly Flame-Retardant Cellulose Nanofibril Aerogels by Incorporating Sodium Bicarbonate. *ACS Applied Materials and Interfaces*, *10*, 27407–27415.

Feng, J., Le, D., Nguyen, S. T., Tan Chin Nien, V., Jewell, D., & Duong, H. M. (2016). Silica–cellulose hybrid aerogels for thermal and acoustic insulation applications. *Colloids and Surfaces A: Physicochemical and Engineering Aspects*, *506*, 298–305.

Follmann, H. D. M., Oliveira, O. N., Martins, A. C., Lazarin-Bidóia, D., Nakamura, C. V., Rubira, A. F., Silva, R., & Asefa, T. (2020). Nanofibrous silica microparticles/polymer hybrid aerogels for sustained delivery of poorly water-soluble camptothecin. *Journal of Colloid and Interface Science*, *567*, 92–102.

Fu, J., Wang, S., He, C., Lu, Z., Huang, J., & Chen, Z. (2016). Facilitated fabrication of high strength

975 silica aerogels using cellulose nanofibrils as scaffold. *Carbohydrate Polymers*, *147*, 89–96.
976 Ganesan, K., Budtova, T., Ratke, L., Gurikov, P., Baudron, V., Preibisch, I., Niemeyer, P., Smirnova, I.,
977 & Milow, B. (2018). Review on the production of polysaccharide aerogel particles. *Materials*, *11*,
978 1–37.
979 García-González, C. A., Uy, J. J., Alnaief, M., & Smirnova, I. (2012). Preparation of tailor-made starch-
980 based aerogel microspheres by the emulsion-gelation method. *Carbohydrate Polymers*, *88*,
981 1378–1386.
982 Ge, X., Shan, Y., Wu, L., Mu, X., Peng, H., & Jiang, Y. (2018). High-strength and morphology-controlled
983 aerogel based on carboxymethyl cellulose and graphene oxide. *Carbohydrate Polymers*, *197*,
984 277–283.
985 Glenn, G. M., & Irving, D. W. (1995). Starch-Based Microcellular Foams. *American Association of*
986 *Cereal Chemists*, *72*, 155–161.
987 Gibson, L. J., & Ashby, M. F. (1999). Cellular Solids. Structure and Properties (2nd ed.). New York:
988 Cambridge University Press, pp: 184−192.
989 Gross, J., Reichenauer, G., & Fricke, j. (1988). Mechanical properties of SiO_2 - aerogels. *J. Phys. D:*
990 *Appl. Phys.*, *21*, 1447–1451.
991 Groult, S., & Budtova, T. (2018a). Thermal conductivity/structure correlations in thermal super-insulating
992 pectin aerogels. *Carbohydrate Polymers*, *196*, 73–81.
993 Groult, S., & Budtova, T. (2018b). Tuning structure and properties of pectin aerogels. *European Polymer*
994 *Journal*, *108*, 250–261.
995 Guerrero-Alburquerque, N., Zhao, S., Adilien, N., Koebel, M. M., Lattuada, M., & Malfait, W. J. (2020).
996 Strong, Machinable, and Insulating Chitosan-Urea Aerogels: Toward Ambient Pressure Drying of

997 Biopolymer Aerogel Monoliths. *ACS Applied Materials and Interfaces*, *12*, 22037–22049.
998 Guo, L., Chen, Z., Lyu, S., Fu, F., & Wang, S. (2018). Highly flexible cross-linked cellulose nanofibril
999 sponge-like aerogels with improved mechanical property and enhanced flame retardancy.
1000 *Carbohydrate Polymers*, *179*, 333–340.
1001 Guo, W., Wang, X., Zhang, P., Liu, J., Song, L., & Hu, Y. (2018). Nano-fibrillated cellulose-hydroxyapatite
1002 based composite foams with excellent fire resistance. *Carbohydrate Polymers*, *195*, 71–78.
1003 Gupta, P., Verma, C., & Maji, P. K. (2019). Flame retardant and thermally insulating clay based aerogel
1004 facilitated by cellulose nanofibers. *Journal of Supercritical Fluids*, *152*, 104537.
1005 Gurikov, P., Raman, S. P., Weinrich, D., Fricke, M., & Smirnova, I. (2015). A novel approach to alginate
1006 aerogels: Carbon dioxide induced gelation. *RSC Advances*, *5*, 7812–7818.
1007 Han, Y., Zhang, X., Wu, X., & Lu, C. (2015). Flame Retardant, Heat Insulating Cellulose Aerogels from
1008 Waste Cotton Fabrics by in Situ Formation of Magnesium Hydroxide Nanoparticles in Cellulose
1009 Gel Nanostructures. *ACS Sustainable Chemistry and Engineering*, *3*, 1853–1859.
1010 Hayase, G., Kanamori, K., Abe, K., Yano, H., Maeno, A., Kaji, H., & Nakanishi, K. (2014).
1011 Polymethylsilsesquioxane-cellulose nanofiber biocomposite aerogels with high thermal insulation,
1012 bendability, and superhydrophobicity. *ACS Applied Materials and Interfaces*, *6*, 9466–9471.
1013 Hayase, G., Kanamori, K., Maeno, A., Kaji, H., & Nakanishi, K. (2016). Dynamic spring-back behavior
1014 in evaporative drying of polymethylsilsesquioxane monolithic gels for low-density transparent
1015 thermal superinsulators. *Journal of Non-Crystalline Solids*, *434*, 115–119.
1016 Hemberger, F., Weis, S., Reichenauer, G., & Ebert, H. P. (2009). Thermal transport properties of
1017 functionally graded carbon aerogels. *International Journal of Thermophysics*, *30*, 1357–1371.
1018 Jamart-Grégoire, B., Son, S., Allix, F., Felix, V., Barth, D., Jannot, Y., Pickaert, G., & Degiovanni, A.

(2016). Monolithic organic aerogels derived from single amino-acid based supramolecular gels: Physical and thermal properties. *RSC Advances*, *6*, 102198–102205.

Jaxel, J., Markevicius, G., Rigacci, A., & Budtova, T. (2017). Thermal superinsulating silica aerogels reinforced with short man-made cellulose fibers. *Composites Part A: Applied Science and Manufacturing*, *103*, 113–121.

Jiménez-Saelices, C., Seantier, B., Cathala, B., & Grohens, Y. (2017). Spray freeze-dried nanofibrillated cellulose aerogels with thermal superinsulating properties. *Carbohydrate Polymers*, *157*, 105–113.

Jiménez-Saelices, C., Seantier, B., Grohens, Y., & Capron, I. (2018). Thermal Superinsulating Materials Made from Nanofibrillated Cellulose-Stabilized Pickering Emulsions. *ACS Applied Materials and Interfaces*, *10*, 16193–16202.

Karadagli, I., Schulz, B., Schestakow, M., Milow, B., Gries, T., & Ratke, L. (2015). Production of porous cellulose aerogel fibers by an extrusion process. *Journal of Supercritical Fluids*, *106*, 105–114.

Kobayashi, Y., Saito, T., & Isogai, A. (2014). Aerogels with 3D ordered nanofiber skeletons of liquid-crystalline nanocellulose derivatives as tough and transparent insulators. *Angewandte Chemie - International Edition*, *53*, 10394–10397.

Koebel, M. M., Huber, L., Zhao, S., & Malfait, W. J. (2016). Breakthroughs in cost-effective, scalable production of superinsulating, ambient-dried silica aerogel and silica-biopolymer hybrid aerogels: from laboratory to pilot scale. *Journal of Sol-Gel Science and Technology*, *79*, 308–318.

Koebel, M., Rigacci, A., & Achard, P. (2012). Aerogel-based thermal superinsulation: An overview. *Journal of Sol-Gel Science and Technology*, *63*, 315–339.

Korhonen, O., & Budtova, T. (2020). All-cellulose composite aerogels and cryogels. *Composites Part A: Applied Science and Manufacturing*, *137*, 106027.

1041 Laskowski, J., Milow, B., & Ratke, L. (2015). The effect of embedding highly insulating granular aerogel
1042 in cellulosic aerogel. *Journal of Supercritical Fluids*, *106*, 93–99.
1043 Lavoine, N., & Bergström, L. (2017). Nanocellulose-based foams and aerogels: Processing, properties,
1044 and applications. *Journal of Materials Chemistry A*, *5*, 16105–16117.
1045 Lazzari, L. K., Perondi, D., Zampieri, V. B., Zattera, A. J., & Santana, R. M. C. (2019). Cellulose/biochar
1046 aerogels with excellent mechanical and thermal insulation properties. *Cellulose*, *26*, 9071–9083.
1047 Li, T., Song, J., Zhao, X., Yang, Z., Pastel, G., Xu, S., Jia, C., Dai, J., Dai, C., Gong, A., Jiang, F., Yao,
1048 Y., Fan, T., Yang, B., Wågberg, L., Yang, R., & Hu, L. (2018). Anisotropic, lightweight, strong, and
1049 super thermally insulating nanowood with naturally aligned nanocellulose. *Science Advances*, *4*,
1050 1–10.
1051 Lim, M. B., Ganas, A. S., Hanson, J. L., Zhou, X., Hellner, B., Manandhar, S., Gariepy, R. E., Baneyx,
1052 F., Wilbur, D. S., & Pauzauskie, P. J. (2020). Crystalline loading of lipophilic Coenzyme Q10
1053 pharmaceuticals within conjugated carbon aerogel derivatives. *Carbon*, *164*, 451–458.
1054 Lin, D., Yuen, P. Y., Liu, Y., Liu, W., Liu, N., Dauskardt, R. H., & Cui, Y. (2018). A Silica-Aerogel-
1055 Reinforced Composite Polymer Electrolyte with High Ionic Conductivity and High Modulus.
1056 *Advanced Materials*, *30*. 1802661.
1057 Lu, X., Arduini-Schuster, M. C., Kuhn, J., Nilsson, O., Fricke, J., & Pekala, R. W. (1992). Thermal
1058 conductivity of monolithic organic aerogels. *Science*, *255*, 971–972.
1059 Lu, Xianping, Nilsson, O., Fricke, J., & Pekala, R. W. (1993). Thermal and electrical conductivity of
1060 monolithic carbon aerogels. *Journal of Applied Physics*, *73*, 581–584.
1061 Lu, Y., Wu, H., & Chen, Q. (2015). Facile preparation of fracture-free pectin/clay aerogel monoliths.
1062 *Materials Research Innovations*, *19*, S246–S251.

Maleki, H., Montes, S., Hayati-Roodbari, N., Putz, F., & Huesing, N. (2018). Compressible, Thermally Insulating, and Fire Retardant Aerogels through Self-Assembling Silk Fibroin Biopolymers Inside a Silica Structure - An Approach towards 3D Printing of Aerogels. *ACS Applied Materials and Interfaces*, *10*, 22718–22730.

Maleki, H., Whitmore, L., & Hüsing, N. (2018). Novel multifunctional polymethylsilsesquioxane-silk fibroin aerogel hybrids for environmental and thermal insulation applications. *Journal of Materials Chemistry A*, *6*, 12598–12612.

Markevicius, G., Ladj, R., Niemeyer, P., Budtova, T., & Rigacci, A. (2017). Ambient-dried thermal superinsulating monolithic silica-based aerogels with short cellulosic fibers. *Journal of Materials Science*, *52*, 2210–2221.

IUPAC (2014) Compendium of Chemical Terminology, 2nd ed. (the "Gold Book"). Compiled by McNaught AD, Wilkinson A. Blackwell Scientific Publications, Oxford (1997). XML on ‐ line corrected version: http://goldbook.iupac.org (2006) created by M. Nic, J. Jirat, B. Kosata; updates compiled by A. Jenkins. ISBN 0 ‐ 9678550 ‐ 9 ‐ 8. https://doi. org/10.1351/goldbook. Last update 2014 ‐ 02 ‐ 24; version: 2.3.3.

Mi, Q. Y., Ma, S. R., Yu, J., He, J. S., & Zhang, J. (2016). Flexible and Transparent Cellulose Aerogels with Uniform Nanoporous Structure by a Controlled Regeneration Process. *ACS Sustainable Chemistry and Engineering*, *4*, 656–660.

Munier, P., Apostolopoulou-Kalkavoura, V., Persson, M., & Bergström, L. (2020). Strong silica-nanocellulose anisotropic composite foams combine low thermal conductivity and low moisture uptake. *Cellulose*, *27*, 10825–10836.

Nešić, A., Gordić, M., Davidović, S., Radovanović, Ž., Nedeljković, J., Smirnova, I., & Gurikov, P. (2018).

Pectin-based nanocomposite aerogels for potential insulated food packaging application. *Carbohydrate Polymers*, *195*, 128–135.

Nguyen, S. T., Feng, J., Ng, S. K., Wong, J. P. W., Tan, V. B. C., & Duong, H. M. (2014). Advanced thermal insulation and absorption properties of recycled cellulose aerogels. *Colloids and Surfaces A: Physicochemical and Engineering Aspects*, *445*, 128–134.

Ookuna, S., Igarashi, K., Hara, M., Aso, K., Yoshidone, H., Nakayama, H., Suzuki, K., Nakajima, K. (1993). Porous ion-exchanged fine cellulose particles, method for production thereof, and affinity carrier. USOO5196527A

Pierre, A.C. (2011). Aerogels Handbook (Advances in Sol-Gel Derived Materials and Technologies). In M. A. Aegerter, N. Leventis, & M. M. Koebel (Eds.), History of Aerogels (pp. 3-18). New York Dordrecht Heidelberg London: Springer Science and Business Media.

Pinnow, M., Fink, H. P., Fanter, C., & Kunze, J. (2008). Characterization of highly porous materials from cellulose carbamate. *Macromolecular Symposia*, *262*, 129–139.

Plappert, S. F., Nedelec, J. M., Rennhofer, H., Lichtenegger, H. C., Bernstorff, S., & Liebner, F. W. (2018). Self-Assembly of Cellulose in Super-Cooled Ionic Liquid under the Impact of Decelerated Antisolvent Infusion: An Approach toward Anisotropic Gels and Aerogels. *Biomacromolecules*, *19*, 4411–4422.

Plappert, S. F., Nedelec, J. M., Rennhofer, H., Lichtenegger, H. C., & Liebner, F. W. (2017). Strain Hardening and Pore Size Harmonization by Uniaxial Densification: A Facile Approach toward Superinsulating Aerogels from Nematic Nanofibrillated 2,3-Dicarboxyl Cellulose. *Chemistry of Materials*, *29*, 6630–6641.

Pour, G., Beauger, C., Rigacci, A., & Budtova, T. (2015). Xerocellulose: lightweight, porous and

hydrophobic cellulose prepared via ambient drying. Journal of Materials Science, 50(13), 4526–4535

Qi, J., Xie, Y., Liang, H., Wang, Y., Ge, T., Song, Y., Wang, M., Li, Q., Yu, H., Fan, Z., Liu, S., Wang, Q., Liu, Y., Li, J., Lu, P., & Chen, W. (2019). Lightweight, Flexible, Thermally-Stable, and Thermally-Insulating Aerogels Derived from Cotton Nanofibrillated Cellulose. *ACS Sustainable Chemistry and Engineering*, *7*, 9202–9210.

Raman, S. P., Gurikov, P., & Smirnova, I. (2015). Hybrid alginate based aerogels by carbon dioxide induced gelation: Novel technique for multiple applications. *Journal of Supercritical Fluids*, *106*, 23–33.

Reichenauer, G., Heinemann, U., & Ebert, H. P. (2007). Relationship between pore size and the gas pressure dependence of the gaseous thermal conductivity. *Colloids and Surfaces A: Physicochemical and Engineering Aspects*, *300*, 204–210.

Rennhofer, H., Plappert, S. F., Lichtenegger, H. C., Bernstorff, S., Fitzka, M., Nedelec, J. M., & Liebner, F. W. (2019). Insight into the nanostructure of anisotropic cellulose aerogels upon compression. *Soft Matter*, *15*, 8372–8380.

Robitzer, M., Renzo, F. Di, & Quignard, F. (2011). Natural materials with high surface area. Physisorption methods for the characterization of the texture and surface of polysaccharide aerogels. *Microporous and Mesoporous Materials*, *140*, 9–16.

Rudaz, C. (2013). *Cellulose and Pectin Aerogels : Towards their nano-structuration.* PhD Thesis. CEMEF - Centre de Mise en Forme des Matériaux, Mines ParisTech.

Rudaz, C., Courson, R., Bonnet, L., Calas-Etienne, S., Sallée, H., & Budtova, T. (2014). Aeropectin: Fully biomass-based mechanically strong and thermal superinsulating aerogel.

Biomacromolecules, *15*, 2188–2195.

Sakai, K., Kobayashi, Y., Saito, T., & Isogai, A. (2016). Partitioned airs at microscale and nanoscale: Thermal diffusivity in ultrahigh porosity solids of nanocellulose. *Scientific Reports*, *6*, 1–7.

Schwertfeger, F., Frank, D., & Schmidt, M. (1998). Hydrophobic waterglass based aerogels without solvent exchange or supercritical drying. *Journal of Non-Crystalline Solids*, *225*, 24–29.

Seantier, B., Bendahou, D., Bendahou, A., Grohens, Y., & Kaddami, H. (2016). Multi-scale cellulose based new bio-aerogel composites with thermal super-insulating and tunable mechanical properties. *Carbohydrate Polymers*, *138*, 335–348.

Sehaqui, H., Zimmermann, T., & Tingaut, P. (2014). Hydrophobic cellulose nanopaper through a mild esterification procedure. Cellulose, 21(1), 367–382.

Shang, K., Liao, W., Wang, J., Wang, Y. T., Wang, Y. Z., & Schiraldi, D. A. (2016). Nonflammable Alginate Nanocomposite Aerogels Prepared by a Simple Freeze-Drying and Post-Cross-Linking Method. *ACS Applied Materials and Interfaces*, *8*, 643–650.

Shi, J., Lu, L., Guo, W., Sun, Y., & Cao, Y. (2013). An environment-friendly thermal insulation material from cellulose and plasma modification. *Journal of Applied Polymer Science*, *130*, 3652–3658.

Shi, J., Lu, L., Guo, W., Zhang, J., & Cao, Y. (2013). Heat insulation performance, mechanics and hydrophobic modification of cellulose-SiO_2 composite aerogels. *Carbohydrate Polymers*, *98*, 282–289.

Silva, S. S., Mano, J. F., & Reis, R. L. (2017). Ionic liquids in the processing and chemical modification of chitin and chitosan for biomedical applications. *Green Chemistry*, *19*, 1208–1220.

Song, J., Chen, C., Yang, Z., Kuang, Y., Li, T., Li, Y., Huang, H., Kierzewski, I., Liu, B., He, S., Gao, T., Yuruker, S. U., Gong, A., Yang, B., & Hu, L. (2018). Highly Compressible, Anisotropic Aerogel with

Aligned Cellulose Nanofibers. *ACS Nano*, *12*, 140–147.

Sun, Y., Chu, Y., Wu, W., & Xiao, H. (2021). Nanocellulose-based lightweight porous materials: A review. Carbohydrate Polymers, 255, 117489.

Svensson, A., Larsson, P. T., Salazar-Alvarez, G., & Wågberg, L. (2013). Preparation of dry ultra-porous cellulosic fibres: Characterization and possible initial uses. Carbohydrate Polymers, 92(1), 775–783.

Takeshita, S., & Yoda, S. (2015). Chitosan Aerogels: Transparent, Flexible Thermal Insulators. *Chemistry of Materials*, *27*, 7569–7572.

Tang, L., Zhuang, S., Hong, B., Cai, Z., Chen, Y., & Huang, B. (2019). Synthesis of light weight, high strength biomass-derived composite aerogels with low thermal conductivities. *Cellulose*, *26*, 8699–8712.

Tkalec, G., Knez, Ž., & Novak, Z. (2015). Formation of polysaccharide aerogels in ethanol. *RSC Advances*, *5*, 77362–77371.

Ubeyitogullari, A., & Ciftci, O. N. (2016). Formation of nanoporous aerogels from wheat starch. *Carbohydrate Polymers*, *147*, 125–132.

Wang, D., Peng, H., Yu, B., Zhou, K., Pan, H., Zhang, L., Li, M., Liu, M., Tian, A., & Fu, S. (2020). Biomimetic structural cellulose nanofiber aerogels with exceptional mechanical, flame-retardant and thermal-insulating properties. *Chemical Engineering Journal*, *389*, 124449.

Wang, M., Zhang, B., Ding, J., Xu, N., Bernards, M. T., He, Y., & Shi, Y. (2020). Three-Dimensional Nitrogen-Doped Graphene Aerogel-Supported MnO Nanoparticles as Efficient Electrocatalysts for CO_2 Reduction to CO . *ACS Sustainable Chemistry & Engineering*, *8*, 4983–4994.

Wang, X., Liu, F., Li, Y., Zhang, W., Bai, S., Zheng, X., Huan, J., Cao, G., Yang, T., Wang, M., Jiang, Z.,

Wang, C., & Ho, S. H. (2020). Development of a facile and bi-functional superhydrophobic suspension and its applications in superhydrophobic coatings and aerogels in high-efficiency oil-water separation. *Green Chemistry*, *22*, 7424–7434.

Wang, Y., Wu, K., Xiao, M., Riffat, S. B., Su, Y., & Jiang, F. (2018). Thermal conductivity, structure and mechanical properties of konjac glucomannan/starch based aerogel strengthened by wheat straw. *Carbohydrate Polymers*, *197*, 284–291.

Wang, Y., Uetani, K., Liu, S., Zhang, X., Wang, Y., Lu, P., Wei, T., Fan, Z., Shen, J., Yu, H., Li, S., Zhang, Q., Li, Q., Fan, J., Yang, N., Wang, Q., Liu, Y., Cao, J., Li, J., & Chen, W. (2017). Multifunctional Bionanocomposite Foams with a Chitosan Matrix Reinforced by Nanofibrillated Cellulose. *ChemNanoMat*, *3*, 98–108.

Wicklein, B., Kocjan, A., Salazar-Alvarez, G., Carosio, F., Camino, G., Antonietti, M., & Bergström, L. (2015). Thermally insulating and fire-retardant lightweight anisotropic foams based on nanocellulose and graphene oxide. *Nature Nanotechnology*, *10*, 277–283.

Wiener, M., Reichenauer, G., Braxmeier, S., Hemberger, F., & Ebert, H. P. (2009). Carbon aerogel-based high-temperature thermal insulation. *International Journal of Thermophysics*, *30*, 1372–1385.

Yan, Y., Ge, F., Qin, Y., Ruan, M., Guo, Z., He, C., & Wang, Z. (2020). Ultralight and robust aerogels based on nanochitin towards water-resistant thermal insulators. *Carbohydrate Polymers*, *248*, 116755.

Ye, D. D., Wang, T., Liao, W., Wang, H., Zhao, H. B., Wang, Y. T., Xu, S., & Wang, Y. Z. (2019). Ultrahigh-Temperature Insulating and Fire-Resistant Aerogels from Cationic Amylopectin and Clay via a Facile Route. *ACS Sustainable Chemistry and Engineering*, *7*, 11582–11592.

Yildirim, N., Shaler, S. M., Gardner, D. J., Rice, R., & Bousfield, D. W. (2014). Cellulose nanofibril (CNF) reinforced starch insulating foams. *Cellulose*, *21*, 4337–4347.

Zhang, G., Dass, A., Rawashdeh, A. M. M., Thomas, J., Counsil, J. A., Sotiriou-Leventis, C., Fabrizio, E. F., Ilhan, F., Vassilaras, P., Scheiman, D. A., McCorkle, L., Palczer, A., Johnston, J. C., Meador, M. A., & Leventis, N. (2004). Isocyanate-crosslinked silica aerogel monoliths: Preparation and characterization. *Journal of Non-Crystalline Solids*, *350*, 152–164.

Zhang, L. M., Sui, X. L., Zhao, L., Huang, G. S., Gu, D. M., & Wang, Z. B. (2017). Three-dimensional hybrid aerogels built from graphene and polypyrrole-derived nitrogen-doped carbon nanotubes as a high-efficiency Pt-based catalyst support. *Carbon*, *121*, 518–526.

Zhang, S., Feng, J., Feng, J., Jiang, Y., & Li, L. (2018). Ultra-low shrinkage chitosan aerogels trussed with polyvinyl alcohol. *Materials and Design*, *156*, 398–406.

Zhang, X., Zhao, X., Xue, T., Yang, F., Fan, W., & Liu, T. (2020). Bidirectional anisotropic polyimide/bacterial cellulose aerogels by freeze-drying for super-thermal insulation. *Chemical Engineering Journal*, *385*, 123963.

Zhao, H. B., Chen, M., & Chen, H. B. (2017). Thermally Insulating and Flame-Retardant Polyaniline/Pectin Aerogels. *ACS Sustainable Chemistry and Engineering*, *5*, 7012–7019.

Zhao, S., Malfait, W. J., Demilecamps, A., Zhang, Y., Brunner, S., Huber, L., Tingaut, P., Rigacci, A., Budtova, T., & Koebel, M. M. (2015). Strong, Thermally Superinsulating Biopolymer-Silica Aerogel Hybrids by Cogelation of Silicic Acid with Pectin. *Angewandte Chemie - International Edition*, *54*, 14282–14286.

Zhao, S., Malfait, W. J., Guerrero-Alburquerque, N., Koebel, M. M., & Nyström, G. (2018). Biopolymer Aerogels and Foams: Chemistry, Properties, and Applications. *Angewandte Chemie -*

International Edition, *57*, 7580–7608.

Zhao, S., Malfait, W. J., Jeong, E., Fischer, B., Zhang, Y., Xu, H., Angelica, E., Risen, W. M., Suggs, J. W., & Koebel, M. M. (2016). Facile One-Pot Synthesis of Mechanically Robust Biopolymer-Silica Nanocomposite Aerogel by Cogelation of Silicic Acid with Chitosan in Aqueous Media. *ACS Sustainable Chemistry and Engineering*, *4*, 5674–5683.

Zhao, S., Zhang, Z., Sèbe, G., Wu, R., Rivera Virtudazo, R. V., Tingaut, P., & Koebel, M. M. (2015). Multiscale assembly of superinsulating silica aerogels within silylated nanocellulosic scaffolds: Improved mechanical properties promoted by nanoscale chemical compatibilization. *Advanced Functional Materials*, *25*, 2326–2334.

Zhou, G., Kim, N. R., Chun, S. E., Lee, W., Um, M. K., Chou, T. W., Islam, M. F., Byun, J. H., & Oh, Y. (2018). Highly porous and easy shapeable poly-dopamine derived graphene-coated single walled carbon nanotube aerogels for stretchable wire-type supercapacitors. *Carbon*, *130*, 137–144.

Zhou, S., Apostolopoulou-Kalkavoura, V., Tavares da Costa, M. V., Bergström, L., Strømme, M., & Xu, C. (2020). Elastic Aerogels of Cellulose Nanofibers@Metal–Organic Frameworks for Thermal Insulation and Fire Retardancy. *Nano-Micro Letters*, *12*, 1–13.

Zhou, X., Jin, H., Xu, T., Wang, J., Zhu, Y., Ding, S., Hu, T., Yun, S., & Chen, J. (2020). Excellent flame retardant and thermal insulated palygorskite/wood fiber composite aerogels with improved mechanical properties. *Applied Clay Science*, *184*, 105402.

Zhu, F. (2019). Starch based aerogels: Production, properties and applications. *Trends in Food Science and Technology*, *89*, 1–10.

Zhu, J., Xiong, R., Zhao, F., Peng, T., Hu, J., Xie, L., Xie, H., Wang, K., & Jiang, C. (2020). Lightweight, High-Strength, and Anisotropic Structure Composite Aerogel Based on Hydroxyapatite

Nanocrystal and Chitosan with Thermal Insulation and Flame Retardant Properties. *ACS Sustainable Chemistry and Engineering*, *8*, 71–83.

Zou, F., & Budtova, T. (2020). Tailoring the morphology and properties of starch aerogels and cryogels via starch source and process parameter. *Carbohydrate Polymers*, *255*, 117344.

Zou, F., Peng, L., Fu, W., Zhang, J., & Li, Z. (2015). Flexible superhydrophobic polysiloxane aerogels for oil-water separation via one-pot synthesis in supercritical CO_2. *RSC Advances*, *5*, 76346–76351.

Zu, G., Shen, J., Wang, W., Zou, L., Lian, Y., Zhang, Z., Liu, B., & Zhang, F. (2014). Robust, highly thermally stable, core-shell nanostructured metal oxide aerogels as high-temperature thermal superinsulators, adsorbents, and catalysts. Chemistry of Materials, 26(19), 5761–5772.

Supporting Information

Polysaccharide-based aerogels for thermal insulation and superinsulation: an overview

Fangxin Zou, Tatiana Budtova*

MINES ParisTech, PSL Research University, Center for Materials Forming (CEMEF), UMR CNRS 7635, CS 10207, 06904 Sophia Antipolis, France

*Corresponding author: Tatiana Budtova, Tatiana.budtova@mines-paristech.fr

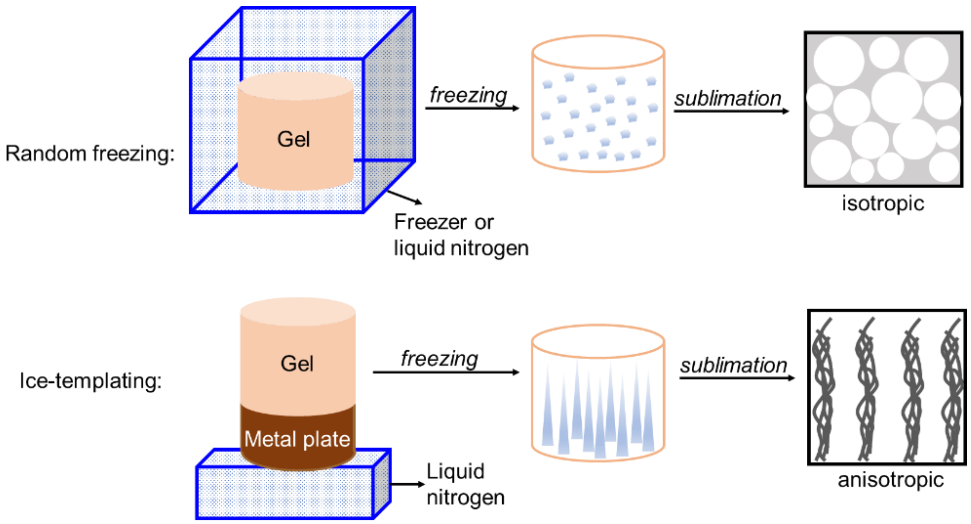

Figure S1.

Schematic presentation of random freezing and ice-templating methods.

1271

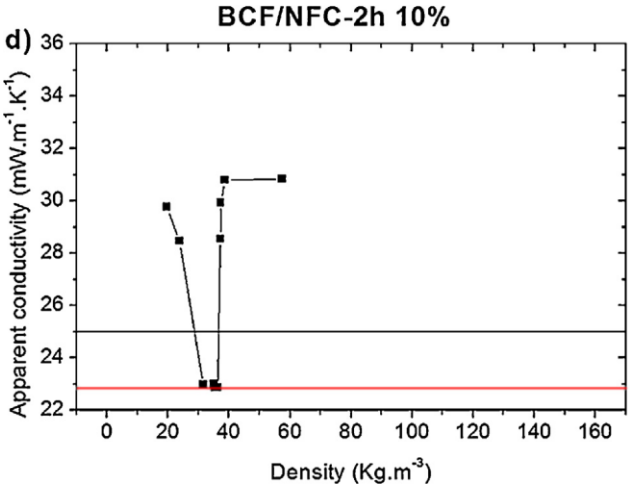

Figure S2.

Example of U-shape conductivity-density dependence for freeze-dried bleached cellulose fibers mixed with CNF. Reprinted from Carbohydrate Polymers, Vol 138, Seantier, B., Bendahou, D., Bendahou, A., Grohens, Y., & Kaddami, H., Multi-scale cellulose based new bio-aerogel composites with thermal super-insulating and tunable mechanical properties, Pages 335–348, Copyright 2016, with permission from Elsevier

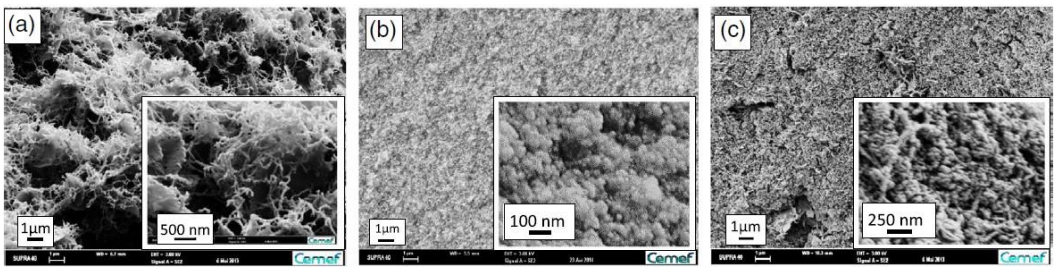

Figure S3.

Aerogels based on tritylcellulose (a), polyethoxydisiloxane (b) and tritylcellulose/polyethoxydisiloxane (c). Reprinted from Journal of Non-Crystalline Solids, Vol 452, Demilecamps, A., Alves, M., Rigacci, A., Reichenauer, G., & Budtova, T., Nanostructured interpenetrated organic-inorganic aerogels with thermal superinsulating properties, Pages 259–265, Copyright 2016, with permission from Elsevier

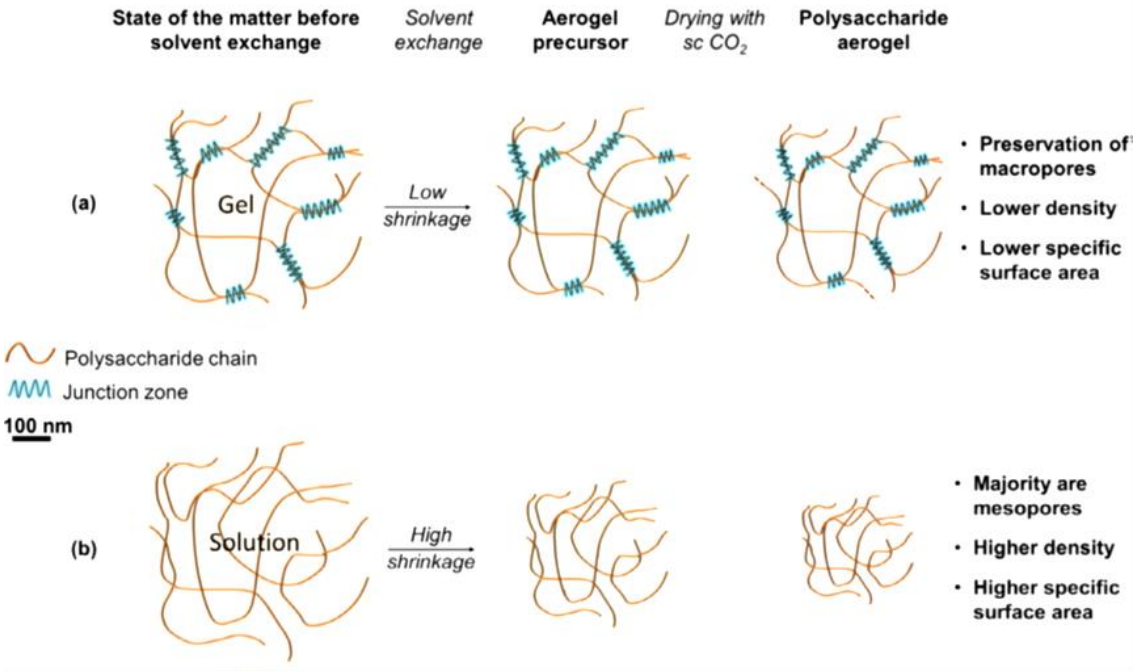

Figure S4.

A schematic presentation of the two main ways of structure formation in pectin aerogels: starting from a gel (a) and from solution via non-solvent induced phase separation (b). Reprinted from European Polymer Journal, Vol 108, Groult, S., & Budtova, T., Tuning structure and properties of pectin aerogels, Pages 250-261, Copyright 2018, with permission from Elsevier

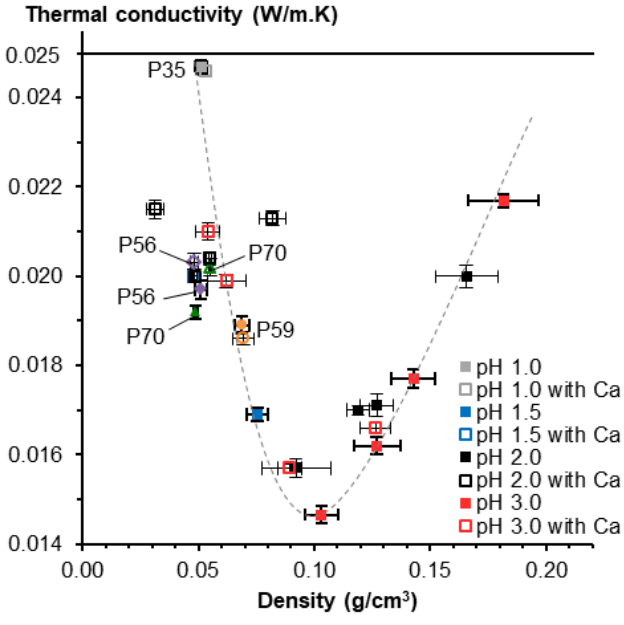

Figure S5.

Thermal conductivity as a function of density for LM pectin aerogel with DE 35 (most of the experimental point) and pectins with various DE: 56% (“P56”, diamonds), 59% (“P59”, circles) and 70% (“P70”, triangles). pH in the legend corresponds to the pH of pectin solution. Solid line is conductivity of air in ambient conditions; dashed line is given to guide the eye. Reprinted from Carbohydrate Polymers, Vol 196, Groult, S. & Budtova, T. Thermal conductivity/structure correlations in thermal super-insulating pectin aerogels, Pages 73-81, Copyright 2018, with permission from Elsevier.

References:

Demilecamps, A., Alves, M., Rigacci, A., Reichenauer, G., & Budtova, T. (2016). Nanostructured interpenetrated organic-inorganic aerogels with thermal superinsulating properties. *Journal of Non-Crystalline Solids*, *452*, 259–265.

Groult, S., & Budtova, T. (2018a). Tuning structure and properties of pectin aerogels. *European Polymer Journal*, *108*, 250–261.

Groult, S., & Budtova, T. (2018b). Thermal conductivity/structure correlations in thermal super-insulating pectin aerogels. *Carbohydrate Polymers*, *196*, 73–81.

Seantier, B., Bendahou, D., Bendahou, A., Grohens, Y., & Kaddami, H. (2016). Multi-scale cellulose based new bio-aerogel composites with thermal super-insulating and tunable mechanical properties. *Carbohydrate Polymers*, *138*, 335–348.